LT-XFD_CDR_XPD-00124

NSLS-II Project

CONCEPTUAL DESIGN REPORT for the

SUBMICRON RESOLUTION X-RAY SPECTROSCOPY (SRX) BEAMLINE AT NSLS-II

final draft Sep 2009

Intentionally blank.

Approvals and Reviewers

Compiled by	**Signature**	**Date**
Juergen Thieme, Beamline Scientist		
Approved		
Qun Shen, XFD Director, NSLS-II		
Reviewers		
Antonio Lanzirotti, BAT Spokesperson, signing on behalf of the BAT		
Andy Broadbent, Beamlines Manager		
Nicholas Gmür, ESH Coordinator, NSLS-II		
Sushil Sharma, Mechanical Engineering Group Leader, NSLS-II		

Document Updates

The Conceptual Design Report for the Submicron Resolution X-ray Spectroscopy (SRX) beamline at NSLS-II is a controlled document, revised under change control.

Version No.	Date	Changes made
A	9/18/2009	Initial draft
1	10/1/2009	Final draft, submitted to BAT

Intentionally blank.

Contents

1 INTRODUCTION 1

1.1 SCIENTIFIC REQUIREMENTS 1
1.2 BEAMLINE ADVISORY TEAM (BAT) 2
1.3 REPRESENTATIVE EXPERIMENTS 2
1.4 COMPARISON TO OTHER INSTRUMENTS 6

2 BEAMLINE LAYOUT 8

2.1 OVERVIEW 8
2.2 INSERTION DEVICE AND LOW β STRAIGHT SECTION AND OPERATION MODES 10
2.3 FRONT END 13
2.4 OPTICAL LAYOUT 13
2.5 HIGH HEATLOAD OPTICS 17
2.6 RAY TRACING 28
2.7 LIST OF MAJOR COMPONENTS 32

3 END STATION INSTRUMENTATION 39

3.1 HUTCH MECHANICAL, ENVIRONMENTAL AND UTILITIES REQUIREMENT 39
3.2 SAMPLE MOUNTING, ENVIRONMENTS AND MANIPULATION 40
3.3 DETECTORS 42

4 SPECIAL BEAMLINE REQUIREMENTS 44

5 FUTURE UPGRADE OPTIONS 44

APPENDIX 1: SCHEDULE 45

APPENDIX 2: REFERENCE DRAWINGS 47

Acronyms

FEA	Front End Aperture
FOE	First Optical Enclosure
FWHM	Full Width at Half Minimum
HMP	Horizontal Mirror Pair
IVU	In-Vacuum Undulator
KB	Kirkpatrick-Baez
MLL	Multi Layer Laue Lens
OA	Optical Aperture
SHS	Secondary Horizontal Source
SHSA	Secondary Horizontal Source Aperture
SRX	Submicron Resolution X-ray Spectroscopy beamline
WBF	White Beam Filter
WBS	White Beam Slit
ZP	Zone Plate

1 INTRODUCTION

1.1 Scientific Requirements

Scientific communities (such as Earth, Environmental, and Life sciences, Hard Condensed Matter and Materials sciences, Chemical and Energy sciences) have all identified analytical resources that must be developed to advance our understanding complex natural and engineered systems that are heterogeneous on the micron to submicron scale. These groups in particular specified a need for higher intensity focused x-ray probes and made it clear in the Letter of Interest they submitted to the NSLS-II Project for the Sub-Micron Resolution X-Ray (SRX) Spectroscopy Beamline, that NSLS-II would provide one of the best sources in the world for such instruments. The research topics these scientific communities hoped to better address using such an instrument require characterization of elemental abundances and speciation in samples that are heterogeneous at the sub-micrometer scale. The targeted scientific issues show a wide gamut of environmental and health issues of high societal impact. Interactions between micro-organisms and minerals control the speciation, migration and toxicity of contaminated materials produced by human activity. Micro-organisms and particulates are likely major players in the cycling of nutrients and metals in the Earth's oceans, processes that can have a significant impact on conditions at the planetary scale, such as global climate change. The properties of airborne particulates can have a profound effect on the toxicity of atmospheric dust introduced to the human body by inhalation. The study of how genetic variations in organisms affect their interactions with contaminant and nutrient metal species in the environment is in its infancy but likely to be greatly advanced with this new technology because of the ability to observe in detail the chemical modifications in organisms caused by genetic modification. Equally significant will be studies of the varied sources, pathways and functions of metals in organisms, in particular their role in human health. Some metals are required for normal metabolic function, with optimal amounts for maximum benefit. Others are only known to cause toxic effects. Metal ions are also used both as treatments for disease and as image contrast agents within the body. Yet, in order to understand at the molecular level how metal ions function in life, disease, and therapy, a multi-dimensional approach is necessary. Such an instrument will allow studies of catalysis and chemical processes at the scale of a single particle using coupled μXAS/μXRD of catalytic particles and interfaces to follow processes such as oxidation. In the materials sciences scientists will be able to research the elemental partitioning in microelectronics and elemental diffusion into microcrystalline domains that occur due to aging of plastics and alloys and tracking redox changes of single particle contaminants in batteries and silicon solar cells.

The SRX sector with its unique combination of high spectral resolution over a very broad energy range and very high beam intensity in a sub-micrometer spot will be a tool very well suited for the study of the scientific issues mentioned above. The design envisions a canted undulator sector that will consist of two beamlines, each optimized for a specific energy range that will allow the scientific community to cover the spectroscopic range they identified was needed for the research. Two beamlines are required to cover the large energy range and spatial resolution of interest in an optimal way. The first beamline is optimized to access higher energy and is included in the initial budget scope for the SRX sector. It will access an energy range of E = 4 keV to E = 25 keV. The second low energy beamline, accessing spectroscopic edges from E = 2 keV to E = 15 keV, will require additional funding to be completed.

The high energy cut-off of E = 25 keV of the first beamline is determined by the energy at which the brightness of the NSLS-II undulators has dropped by approximately two orders of magnitude from that of the third harmonic at closed gap. Also, the K absorption edge of rhodium, the likely mirror coating, will begin to interfere at about E = 23 keV. The low energy cut-off of E = 4 keV is the energy at which the undulator third harmonic is likely to begin. It will still give access to elements down to the Ti K edge.

The low energy cut-off of E = 2 keV of the second beamline is set by the limits of the Si (111) monochromator, while still reaching the K absorption edge of phosphorus. The high-energy cut-off of E = 15 keV is determined by the need to access the LIII absorption edge of lead at E = 13 keV.

1.2 Beamline Advisory Team (BAT)

Peter Eng: Senior Research Associate, University of Chicago
Jeffrey Fitts: Assistant Geochemist, Brookhaven National Laboratory
Chris Jacobsen: Professor, Stony Brook University
Keith Jones: Senior Physicist, Brookhaven National Laboratory
Antonio Lanzirotti (BAT Spokesperson): Senior Research Associate, University of Chicago
Lisa Miller: Biophysical Chemist, Brookhaven National Laboratory
Matt Newville: Senior Research Associate, University of Chicago
Paul Northrup: Associate Environmental Scientist, Brookhaven National Laboratory
Richard Reeder: Professor, Stony Brook University
Mark Rivers: Senior Scientist, University of Chicago
Stephen Sutton: Senior Scientist, University of Chicago
Stefan Vogt: Beamline Scientist, Advanced Photon Source, Argonne National Laboratory
Gayle Woloschak: Professor, Northwestern University

1.3 Representative Experiments

There are a number of research areas where the SRX beamline will enable significant advances. Largely this will be due to the world leading flux density the SRX probes will provide, their unique sub-micrometer x-ray fluorescence and x-ray spectroscopic capabilities and the plan to develop these hard x-ray methodologies as imaging modalities by utilizing both the beamline's optical characteristics and advanced detector technologies. This holds true for both branches of this beamline, the Kirkpatrick-Baez (KB) based instruments as well as the zone plate (ZP) based instrument. Only the KB branch is part of the original scope of the NSLS-II project, however it is expressly desired by the scientific community to establish the ZP branch as contemporary as possible. An exhaustive list of potential experiments that could be conducted on this beamline and their scientific significance is presented in the original Letter of Interest (LOI) submitted by the beamline advisory team (BAT). Some of the experiments discussed in the LOI include:

- How SRX will extend x-ray elemental analysis, spectroscopy, and scattering to spatial resolutions suitable for the analysis of aerosols.
- Applications of coupled sub-micrometer XRF, XAFS and XRD methods to access to the details of microbial-mineral interactions in-situ.
- Sub-micrometer XRF, XAFS and XRD studies of how micro-organisms fixate and cycle carbon and nitrogen in the Earth's oceans using metalloenzymes.
- Evaluation of how specific genes influence the uptake of metals in plants and animals at the cellular level using the highest spatially-resolved XRF and XAFS computed microtomography available *in-vivo*.
- Characterization of how metallic-DNA nanocomposites target individual cells to determine specific localization.
- Sub-micrometer XAFS studies to constrain the speciation of metallic species that may contribute to the oxidative damage of cells from redox processes.

At this point an example of how the unique optical characteristics of the Kirkpatrick-Baez (KB) instrument at the SRX beamline, the advanced energy scanning capabilities of the beamline's monochromator and in-vacuum undulator, and the synergistic development of advanced energy dispersive detectors at BNL will help formulate new methodologies for sub-micrometer hard x-ray spectroscopy. Given the predicted intensity of the KB instrument, many spectroscopic experiments will benefit from being conducted in an 'event driven' or 'image stack' modality utilizing fluorescence detectors that support fast on-the-fly scanning modes working in conjunction with high precision monochromator and undulator energy scanning. This must all be done with suitable feedback to maintain focused beam position on the sample within a few nanometers. A preliminary evaluation of how such experiments can be designed an implemented was conducted by members of the BAT (P. Eng, A. Lanzirotti, and M. Rivers – U. Chicago in collaboration with Emily Knowles and Alexis Templeton – U.C. Boulder) at the

Australian Synchrotron's X-ray Fluorescence Microspectroscopy beamline (5ID). This Kirkpatrick-Baez mirror based beamline shares a great deal of commonality with the proposed design of the KB based instrument at the SRX beamline including a high stability horizontally diffracting monochromator design, the use of a harmonic rejecting horizontally focusing mirror, an in-vacuum undulator that is designed to synchronize with the monochromator to keep the undulator tuned to the maximum of its emission peak, and an evaluation program of a prototype 96-element BNL-CSIRO *Maia* detector system. Photon flux of the 5ID KB instrument at E = 10 keV is ~ $4x10^{12}$ ph/sec. The KB instrument at the SRX beamline is expected to deliver more than a factor of 10 higher flux to the sample in a spot size that is up to a factor of 10 smaller.

This experiment sought to examine the redistribution of metals and changes in metal speciation associated with microbial alteration of deep-sea volcanic glasses. There is considerable interest in understanding the microchemistry of these organisms and their environment since they may constitute a significant fraction of the global biomass (and are thus relevant in modelling climate change) and are relevant to the development of the earliest life on Earth (and potentially models for the evolution of life on other planets). The granular alteration left by these microbes in deep sea basaltic glasses are typically only a few microns in diameter, requiring highly resolved spectroscopic probes for evaluating the chemistry of the alteration products.

Figure 1 shows in the left a plane light photomicrograph of a sample of the Troodos Ophiolite, a 170 million year old sample of obducted oceanic crust. The box marked in blue delineates an area that was compositionally mapped using the prototype *Maia* X-ray fluorescence detector. The dark filamentous areas in the center left of the figure show areas of microbial alteration. An Fe compositional map is shown in the upper right and a composite Fe-Ti-Mn RGB map in the lower right of Figure 1. These maps were collected as on-the-fly continuous scans with a dwell time that translates to 16 msec per pixel at a pixel size of 1.25 µm. The *Maia* detector is operating in an event-driven list mode, counting each individual photon as a function of its energy and motor position. These images, collected over roughly 6 hours, represent almost 1.5 Megapixels of full energy dispersive data. The rapid detector readout coupled with high instrument brightness and precise energy control then allows for Fe K-edge spectroscopy to be conducted in an image stack mode similar to what has been developed by Chris Jacobsen to STXM instruments. The smaller area of the section marked in a red box on the photomicrograph shows one specific area that was interrogated using this image-stack approach. Each individual image in the stack contains 14,400 pixels collected at 16 msec dwell time and a pixel resolution of 1.25 µm. After each image the monochromator and the IVU adjust energy in unison, scanning through the Fe K absorption edge (compare Figure 2) to produce a stack of images from which high-resolution Fe K-edge XANES data can be extracted (Figure 3). This data set required approximately 4 hours of instrument time at this resolution but the planned 384-element *Maia* detector planned for SRX-KB should yield 4x higher data rates. Coupled with the significantly higher brightness of this KB instrument and the stability of the horizontally deflecting monochromator and IVU, it can be expected that this likely will be the most common mode in which sub-micrometer resolution X-ray absorption spectroscopy will be conducted at the beamline.

Figure 4 shows as an example what could be achieved with the zone plate (ZP) branch of the SRX beamline results achieved when studying the annually laminated sediments of a lake in Germany using beamline Id21 at the storage ring ESRF. The top left image is an image taken with an optical microscope, showing the lamination of the sample. This lamination originates from the precipitation of carbonates during summer and early autumn and the sedimentation of clay minerals and organic matter during winter and spring. Such laminae are only preserved, when bioturbation is prevented and thus evidence anoxic conditions. Even though, XANES at the sulfur K-absorption edge was able to determine a different sulfur species distribution in different laminated sediment sections. The lamination is also reproduced when looking at the sample in the X-ray fluorescence light at E = 2490 eV, just above the K-absorption edge of sulfur. Sulfur-rich and sulfur-poor layers alternate. To identify the sulfur speciation within the layers, a sequence of XANES spectra has been taken, following the trajectory from A to B, indicated in the top images. The lower image of Figure 8 is a three-dimensional representation of this set of spectra. It shows, that the amount of reduced sulfur species decreases when going from A to B, whereas the oxidized species gets more prominent.

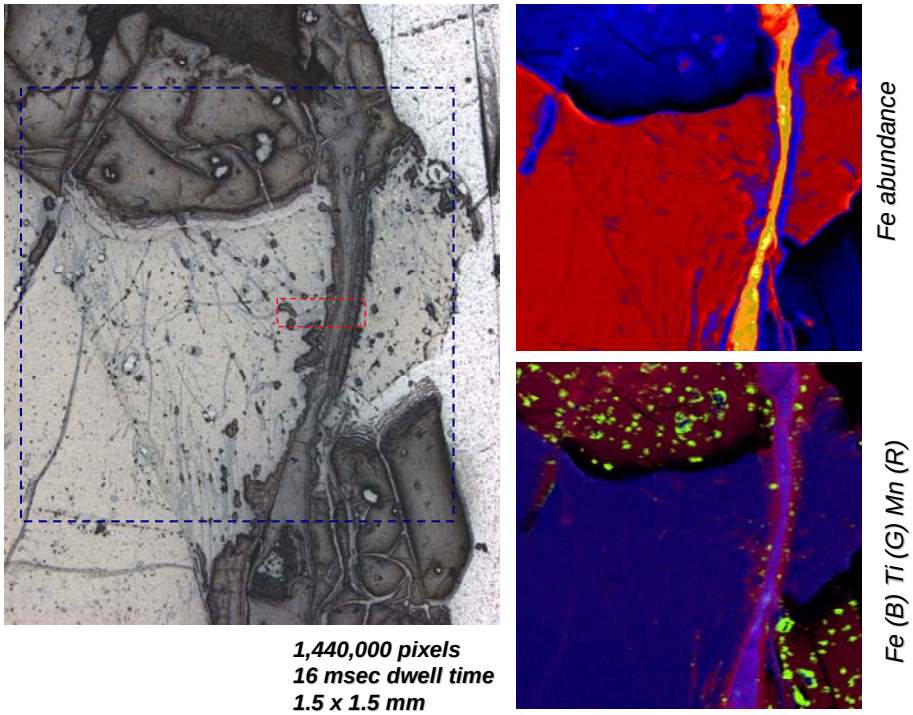

Figure 1. (Left) plane light photomicrograph of a sample of the Troodos Ophiolite, a 170 million-year-old sample of obducted oceanic crust. The box marked in blue delineates an area that was compositionally mapped using the prototype *Maia* X-ray fluorescence detector. The area delineated in red shows where Fe K-edge image stack XANES data were collected. The dark filamentous areas in the center left of the figure show areas of microbial alteration. (Top Right) Fe compositional map of the blue area. (Bottom Right) Composite Fe-Ti-Mn RGB map of the blue area. These were collected as on-the-fly continuous scans with a dwell time that translates to 16 msec per pixel at a pixel size of 1.25 µm.
(Knowles, Templeton, Eng, Lanzirotti, Rivers. Unpublished data)

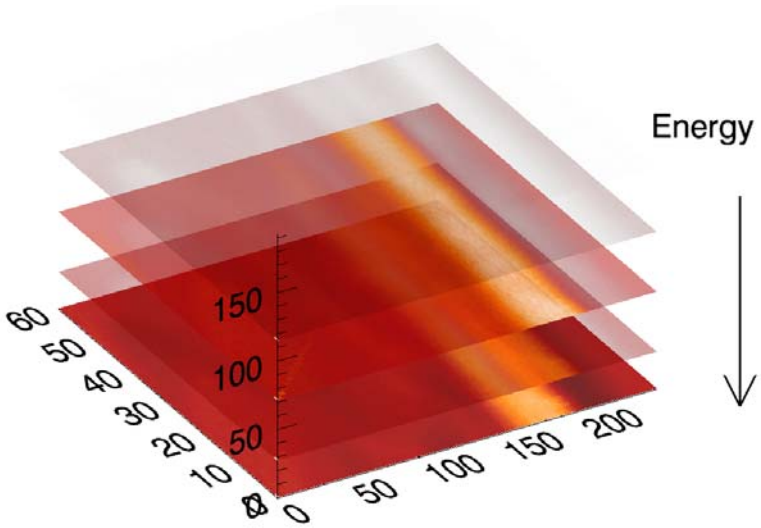

Figure 2. Selected Fe K-edge image stacks as a function of incident beam energy for the area marked in red in Figure 1. (Knowles, Templeton, Eng, Lanzirotti, Rivers. Unpublished data).

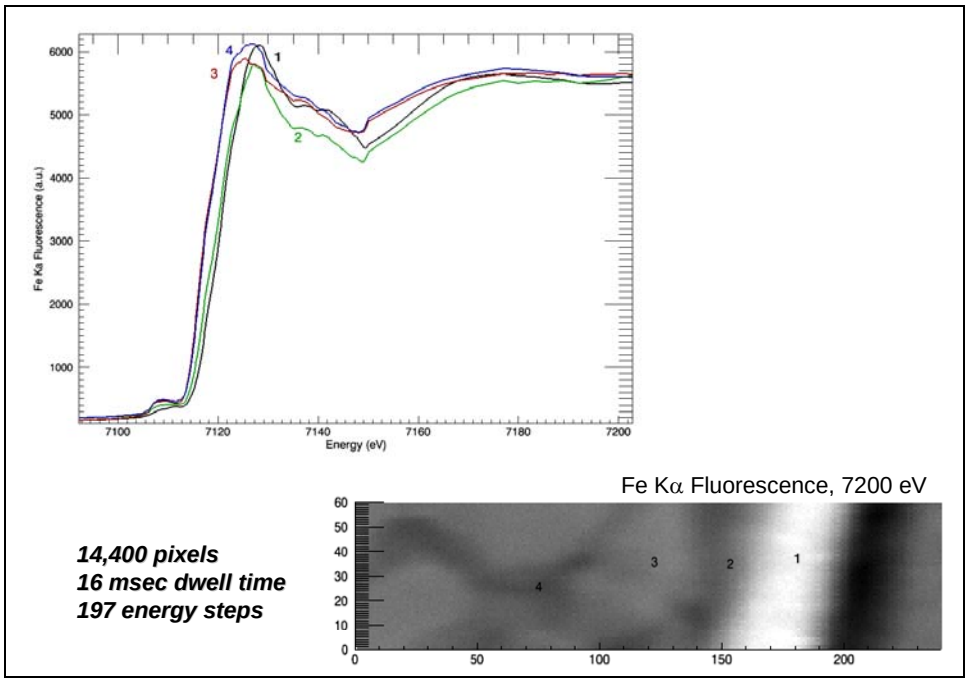

Figure 3. (Bottom) Fe K-edge image stack of the area marked in red in Fig. 1, collected at 7200 eV incident beam energy. Each map contains 14,400 pixels collected with 16 msec dwell time and 1.25 µm pixel resolution. 197 energy steps were collected for the entire stack. (Top) Extracted Fe K-edge XANES spectra from the image stack at pixel locations (1-4) marked on the bottom image. (Knowles, Templeton, Eng, Lanzirotti, Rivers. Unpublished data)

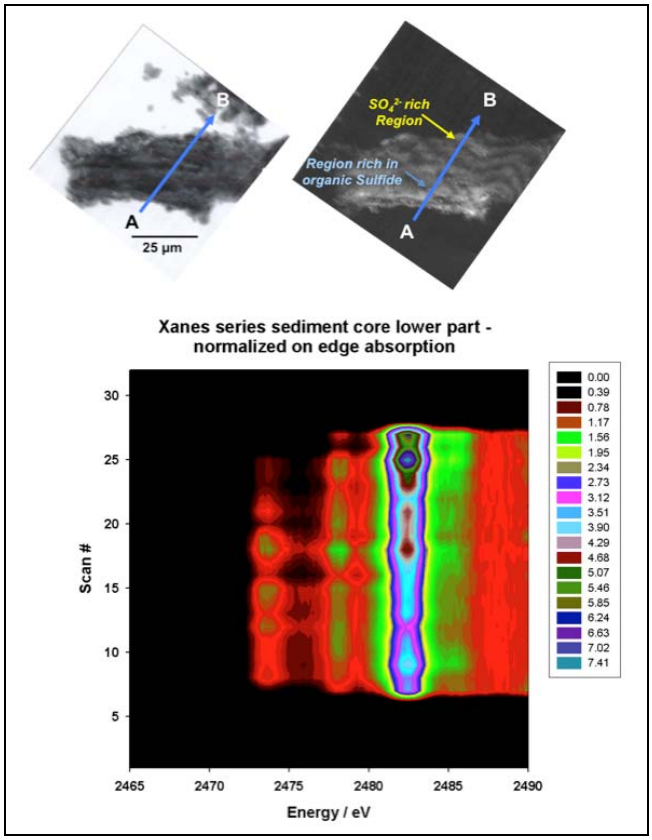

Figure 4. (top left) Optical microscope image of a section of a laminated sediment core from the lake Steisslinger See. (top right) X-ray fluorescence image of the same sediment core taken at E = 2.490 keV, showing the same lamination. (bottom) 3D-representation of the XANES spectra across the sediment core, scan numbers increasing from A to B.

1.4 Comparison to Other Instruments

The following list might be far fom complete but shows exemplary the scientific environment in which the SRX beamline would evolve delivering the highest photon flux in the smallest spot.

1. Beamline ID21 at electron storage ring ESRF in Grenoble, France

   This scanning transmission x-ray microscope is designed for using the spectral range from E = 6.5 keV to E = 18 keV for spectromicroscopy experiments in life, materials and environmental sciences. The instrument is capable of absorption contrast imaging, fluorescence imaging and XANES imaging. Using a zone plate or a KB mirror system as focusing optics the spatial resolution lies in the range of 0.2 – 1 µm.

2. Beamline ID22 at electron storage ring ESRF in Grenoble, France

   This x-ray microprobe scope is designed for using the spectral range from E = 2 keV to E = 7.5 keV. It provides a focused x-ray beam of about 3.5 x 1.5 μm^2 at a flux of up to 10^{12} ph/s. The instrument offers access to absorption, fluorescence and diffraction, fluorescence-tomography, XANES imaging, holography and phase-contrast micro-tomography, focusing optics are KB mirrors and compound refractive lenses.

3. Beamline 2-ID-B at the Advanced Photon Source in Argonne, IL

   This beamline is built for scanning x-ray microscopy and coherent diffraction x-ray microscopy in the energy range from E ≤ 1 keV up to E = 4 keV. Phase contrast, micro-fluorescence imaging and XANES are supported as well as coherent x-ray scattering and diffraction imaging. A photon flux up to 10^9 phot/sec and a spot size of 60 x 60 nm^2 using a Fresnel zone plate can be utilized for experiments.

4. Beamline 2-ID-D at the Advanced Photon Source in Argonne, IL

   That beamline is built for sub-micron high-resolution x-ray imaging studies. Most of the work centers on fluorescence analysis of biological samples and micro-diffraction of a variety of materials. Micro-fluorescence, micro-diffraction and micro-XAFS are available for experiments. The usable x-ray energy ranges from E = 5 keV up to E = 30 keV, flux can be expected as high as 4 x 10^9 phot/sec, the spatial resolution goes down to 0.2 x 0.2 μm^2.

5. Beamline 2-ID-E at the Advanced Photon Source in Argonne, IL

   This beamline is built as a micro-fluorescence imaging station. The energy usable for experiments ranges from E = 7.5 keV up to E = 10 keV. A photon flux up to 5 x 10^9 phot/sec and a spot size of 0.5 x 0.3 μm^2 using a Fresnel zone plate optics can be utilized for experiments.

6. Beamline 13-ID-C,D at the Advanced Photon Source in Argonne, IL

   This beamline is specialized on earth and environmental science research. The reachable energy ranges from E = 4 keV to E = 45 keV. A KB mirror system focuses the beam into a 2 x 2 μm^2 spot with a photon flux of up to 1 x 10^{11} phot/sec. Inelastic x-ray scattering, micro-XAFS, micro - diffraction, x-ray absorption fine structure (XAFS), and micro-fluorescence are supported techniques. High pressure diamond anvil cell and high pressure multi-anvil press (LVP) are available for sample treatment.

7. Beamline 20-ID-B,C at the Advanced Photon Source in Argonne, IL

   This beamline is specialized on material science, environmental science, chemistry and geoscience. When focused using KB mirrors, it covers energy range from E = 4.3 keV to E = 27 keV delivering the beam into a 2 x 2 μm^2 spot with a photon flux of up to 1 x 10^{11} phot/sec. X-ray absorption fine structure (XAFS), surface diffraction, x-ray raman scattering, micro-XAFS, micro-fluorescence time resolved XAFS, and x-ray emission spectroscopy are supported techniques.

8. Beamline X26A at the National Synchrotron Light Source in Brookhaven, NY

The beamline covers an energy range in a focused mode from E = 4 keV to E = 30 eV, using a KB setup, which focuses the monochromatic beam down to 5 µm x 10 µm size. Photon flux is then in the range of 3 x 10^9 phot/sec. The beamline can be utilized as a microprobe and is as well suited for microdiffraction imaging.

9. Beamline X27A at the National Synchrotron Light Source in Brookhaven, NY

The beamline covers an energy range in a focused mode from E = 4.5 keV to E = 32 eV, using a KB setup to focus the monochromatic beam down to 15 µm x 10 µm size. Photon flux is then in the range of 1-5 x 10^9 phot/sec. This beamline is a microprobe being used by researches from environmental science, geoscience, physics, chemistry, and biology.

10. XFM beamline at the Australian Synchrotron Project

The X-ray Fluorescence Microprobe at the Australian Synchrotron is a microprobe station with either a KB mirror system with a spot size down to 2 x 1 μm^2 or a ZP showing a spot size of about 0.06 x 0.06 μm^2. The energy range scales from E = 4.1 keV up to E = 25 keV, the photon flux can reach 4 x 10^{11}phot/sec for the KB and 10^{10} phot/sec for the ZP optics.

11. MicroXAS beamline at the Swiss Light Source

This beamline focuses on x-ray fluorescence imaging and XAS spectroscopy with a spatial resolution in the 1 x 1 μm^2 range. The energies available for experiments range from E = 5 keV up to E = 20 keV. A photon flux up to 2 x 10^{12} phot/s will be delivered.

12. LUCIA beamline at the synchrotron SOLEIL, Gif-sur-Yvette, France

The beamline LUCIA covers the energy range from E = 0.8 keV up to E = 8 keV. It is an x-ray microprobe with capabilities for chemical speciation by x-ray absorption spectroscopy (µXAS) and for elemental mapping by x-ray micro-fluorescence (µXRF). The focusing is done with a "Kirkpatrick-Baez" (KB) reflecting mirrors system, yielding a focal spot of about 2.5 x 2.5 μm^2. A photon flux up to 2 x 10^{11} phot/s can be expected.

2 BEAMLINE LAYOUT

2.1 Overview

The general concept of the SRX beamline is to offer stations where x-ray spectromicroscopy experiments can be performed with a spatial resolution in the sub-micrometer range. The energy range covered should extend from E = 2 keV up to E = 28 keV. This concept will be realized by dividing this beamline into two branches, each served by an optimized, in-vacuum undulator with the two insertion devices arranged in a canted geometry. One branch will be equipped with focusing mirrors in a Kirkpatrick-Baez (KB) setup, aiming at a spatial resolution down to 100 x 100 nm^2, working in the energy range from E = 4.65 keV up to E = 28 keV, and delivering a flux of up to 5 x 10^{12} phot/sec in that spot. The other branch will use a Fresnel zone plate to reach a spatial resolution down to 30 nm in the energy range of E = 2 keV up to E = 15 keV, where the expected flux will be up to 7 x 10^9 phot/sec. Photon flux and spatial resolution in that energy range will be unprecedented as can be seen when comparing these key parameters to similar beamlines as listed on the previous page. The KB branch is a project beamline of the NSLS-II project; the ZP branch is not in the original scope. To ensure that a reasonable design and layout for the latter will be available when an approving decision will be due, the conceptual design of both branches will be found in this report. A schematic view of the sector starting with the two canted undulators and showing major optical components of the two branch lines is seen in Figure 5. Note, that the angle between the two branches is exaggerated for illustration purposes.

The optical layout of the KB-branch is shown in Figure 6. Due to heat load reasons (see chapter 2.5), the double crystal monochromator will be the first optical element downstream of the storage ring shield wall, followed by the horizontally focusing mirror. The Secondary Horizontal Source Aperture will define the source point for the KB mirrors located downstream in the hutch. The KB mirrors will create a demagnified image of this source point as a focal spot through which the sample will be scanned. A variety of detectors will be available for fluorescence, transmission and diffraction measurements.

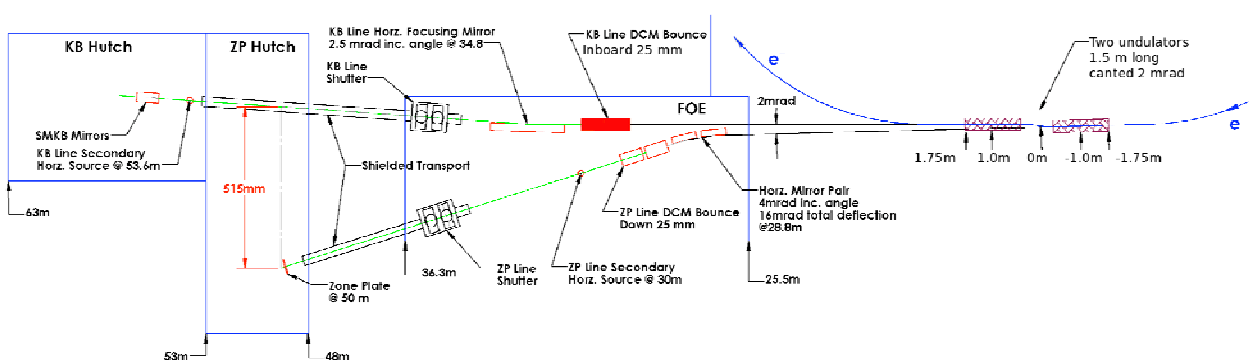

Figure 5. Schematic layout (top view) of the SRX beamline. The angle between the two beamlines is exaggerated for illustration purposes. A canting angle of 2 mrad will be used.

Figure 6 shows a layout of the KB branch of the SRX beamline itself including the hutches, major optical elements and the beam pipes. The first hutch, starting at the ratchet wall, will be the First Optical Enclosure (FOE). Here, the double crystal monochromator and the horizontally focusing mirror of the KB-branch, and the mirror pair and the double-crystal monochromator of the ZP-branch will be found. Due to the canted design of the undulators the x-ray beams for the two branches are very close. Therefore, the optical components for the KB branch have to be constructed in a way that room is available for the x-ray beam feeding the ZP-branch, which may be implemented at a later time. The hutch in the middle will be housing the endstation of the ZP branch, the hutch farthermost downstream will be the place for the endstation of the KB branch, including the KB mirror, the sample holder and the detectors. The Secondary Horizontal Source Aperture will be at the upstream end of this hutch.

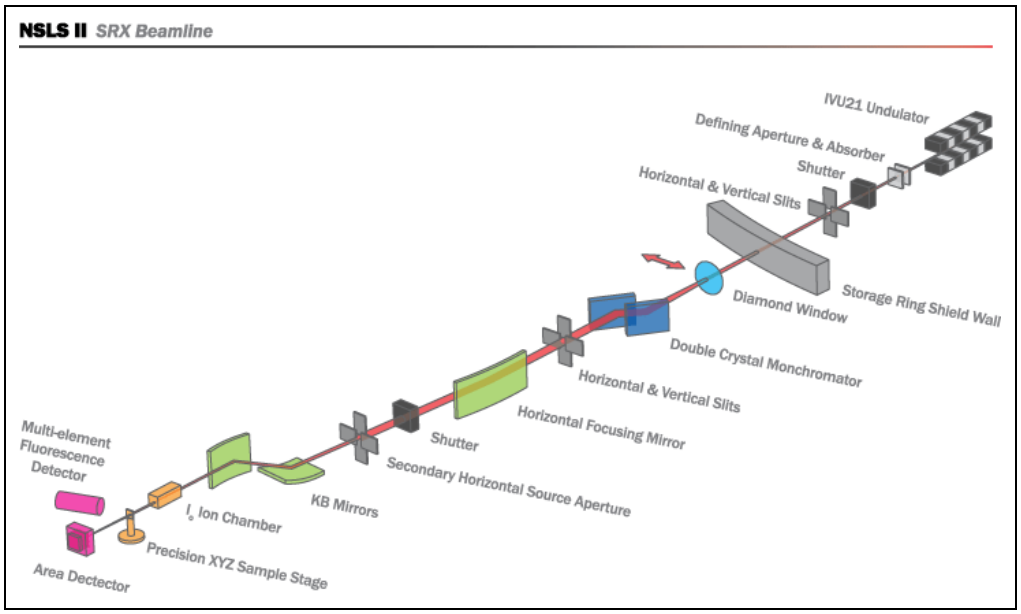

Figure 6. Optical layout of the SRX beamline. Here, only the branch with the Kirkpatrick-Baez mirrors is visible.

Figure 7 shows the layout of the complete beamline, starting at the ratched wall. Three hutches are visible, the first optical enclosure on the right, the zone plate endstation in the middle, and the KB endstation on the left.

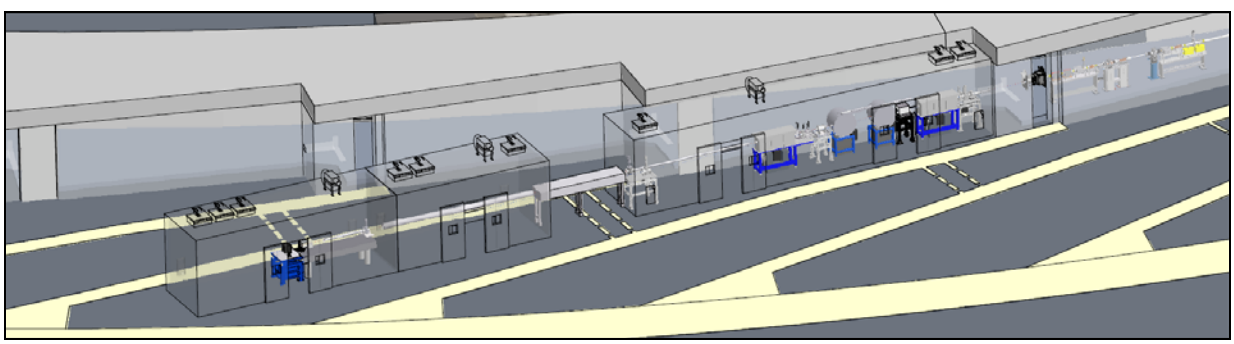

Side view

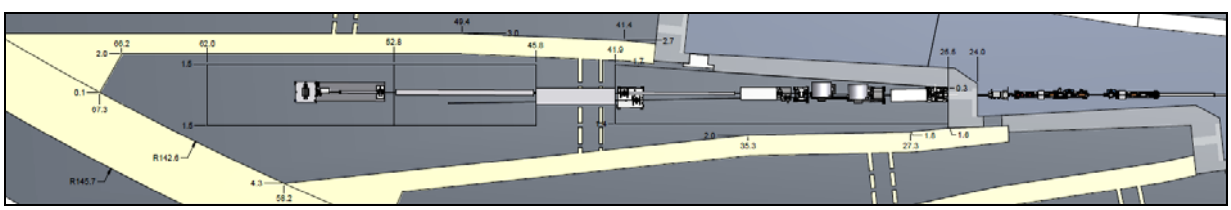

Top view

Figure 7. Beamline layout of the SRX beamline. Hutches (from right to left: FOE, ZP-branch, KB-branch) are indicated.

2.2 Insertion Device and Low β Straight Section and Operation Modes

Table 1. Source Parameters Used for the Calculations within this Document.

Electron Energy	E = 3 GeV
Stored Current	I = 500 mA
Electron Beam Emittance:	
Horizontal	$\varepsilon_x = 0.55 \times 10^{-9}$ m rad
Vertical (1.5% Coupling)	$\varepsilon_y = 8.25 \times 10^{-12}$ m rad
Betatron Function:§	
Horizontal	$\beta_x = 1.5$ m
Vertical	$\beta_y = 0.8$ m
Electron Beam Size:§	
Horizontal	$\sigma_x = 28.7$ μm
Vertical	$\sigma_y = 2.57$ μm
Electron Beam Divergence:§	
Horizontal	$\sigma'_{y\,x} = 19.2$ μrad
Vertical	$\sigma'_{y\,y} = 3.21$ μrad
Intrinsic Photon Size*	$\sigma_r = 1.95$ μm
Intrinsic Photon Divergence*	$\sigma'_y = 4.08$ μrad
Total Photon Source Size:§*	
Horizontal	$\Sigma_x = 28.8$ μm
Vertical	$\Sigma_y = 3.2$ μm
Total Photon Source Divergence:§*	
Horizontal	$\Sigma'_{y\,x} = 28.8$ μrad
Vertical	$\Sigma'_y = 5.19$ μrad

§ Low b straight.
*Quantities evaluated for 12.4keV x-rays and a 3m-long undulator.

The two branches of the SRX beamline are designed for different energy ranges, making the undulator design unusual amongst the suite of insertion devices at NSLS-II. Two undulators in canted geometry on this short (low beta) straight section will serve the two instruments as light sources. As there is the need to do spectroscopy at the titanium K-absorption edge, the specified lowest energy the undulator for the KB branch should reach is E = 4.7 keV. There are a couple of restrictions applied to the choice of the insertion device as a light source for the SRX beamline. The length of the device and the minimum gap have to be adjusted to the limitations stemming from the beta function of the short straight section. A length of 0.5 m minimum has to be removed from the total length of the straight section available for the two undulators to give room for the canting magnets as well as room has to be given to transition pieces and a full canting magnet at the end of the straight, which is also assumed to be 0.5 m long.

The optimized period of an undulator for the KB branch will depend on the gap (itself related to the length of the device through the beta-function restrictions) and the minimum photon energy (E = 4.7 keV). Oleg Tchoubar from NSLS-II has performed the calculations presented below, which are the basis for the decision on the actual undulator for the KB branch.

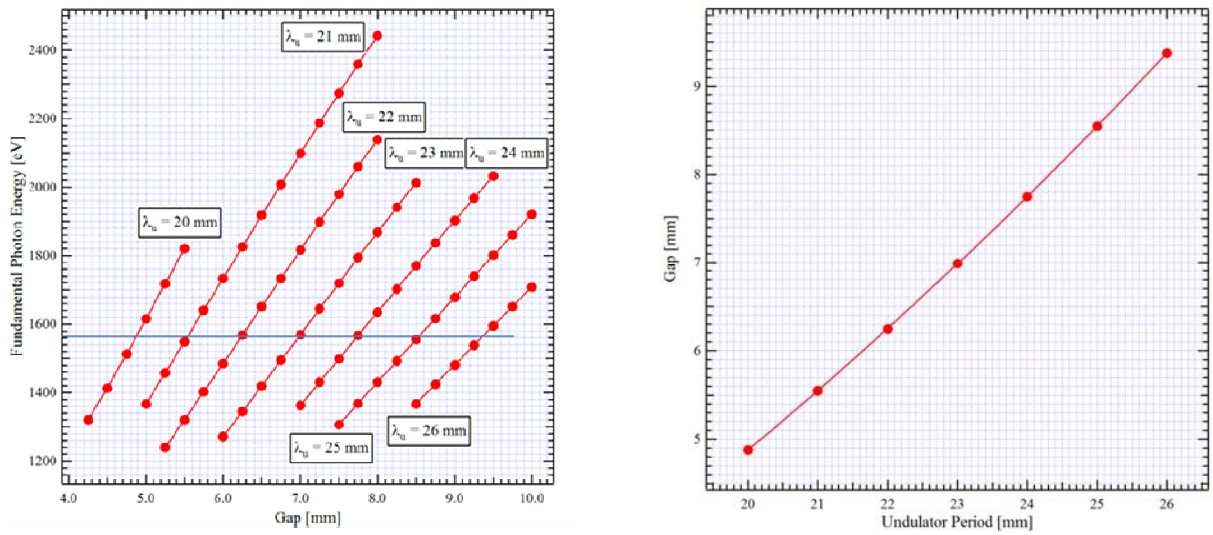

Figure 8. Fundamental photon energy as a function of the gap for different IVU periods (a) and (b) the gap as a function of the IVU period, when the minimum resonant photon energy of the 3rd harmonic is set to E = 4.7 keV.

In Figure 8 the fundamental photon energy as a function of the gap for different in-vacuum undulator (IVU) periods are plotted as well as the gap as a function of the IVU period, when the minimum resonant photon energy of the 3rd harmonic is set to E = 4.7 keV.

The geometry used for the calculations was: Pole Width: 40 mm, Pole Height: 25 mm, Pole Thickness: 3 mm, (for λ_u = 20 mm).Magnet Width: 50 mm, Height: 29 mm, Pole: Va Permendur NEOMAX, Magnet: NdFeB, Br = 1.12 T. These data were supplied from Toshi Tanabe from NSLS-II.

From the graphs in Figure 8 it becomes visible that for a minimum gap of 4.9 mm a period of 20 mm would be allowable, a minimum gap of 5.5 mm would relate to a period of 21 mm and for a gap of 6.2 mm the period would be 22 mm.

The maximum device length for a given minimum gap is determined by the beta function for the straight. Toshi Tanabe from NSLS-II calculated the possible lengths, assuming a canted device placed into a half-straight, as listed in Table 2.

Table 2. Maximum Canted Device Lengths for Given Gaps in a Canted Device Setup.

Gap	Maximum canted device length.
5.0mm	1.25m
5.5mm	1.5m
6.0mm	1.75m
6.26mm	1.85m
6.6mm	2.0m
7.2mm	2.25m

As a result of these calculations three realistic possibilities have been studied more thoroughly, an undulator with 20 mm period and 1.25 m length at a gap of 4.9 mm, an undulator with 21 mm period and 5.5 mm gap and 1.5 m length, and an undulator with 22 mm period and 6.2 mm gap and 1.8 m length. For these further calculations the center of the device is located approximately 1m from the center of the low-beta straight.

Figure 9 shows the spectral flux in phot/sec/0.1%BW of the three possible configurations at odd harmonics as a function of photon energy, and Figure 10 shoes for the same configurations the calculated spectral flux through an aperture of 0.1 x 0.1 mrad^2 at minimal gap.

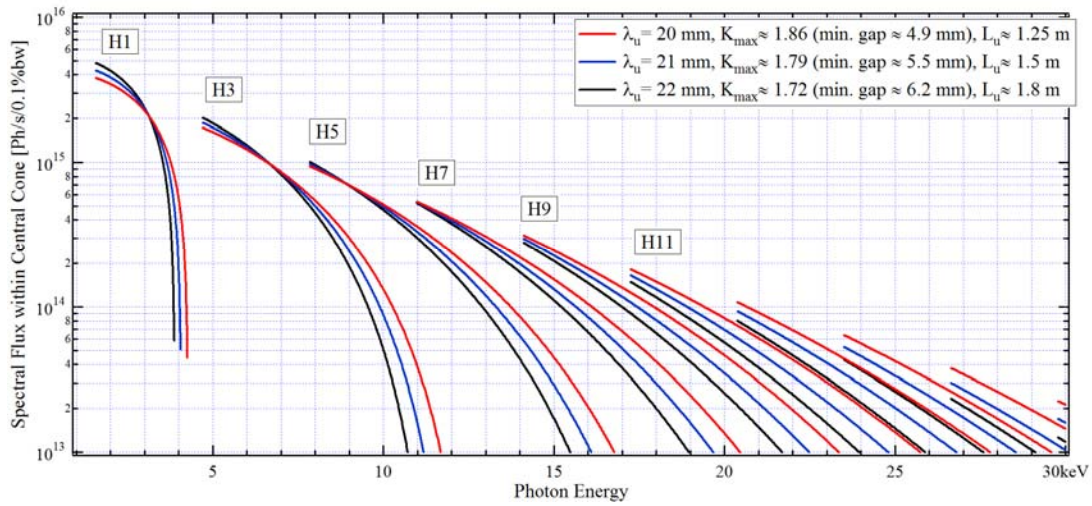

Figure 9. Spectral flux at odd harmonics for three undulator setups as seen in the legend.

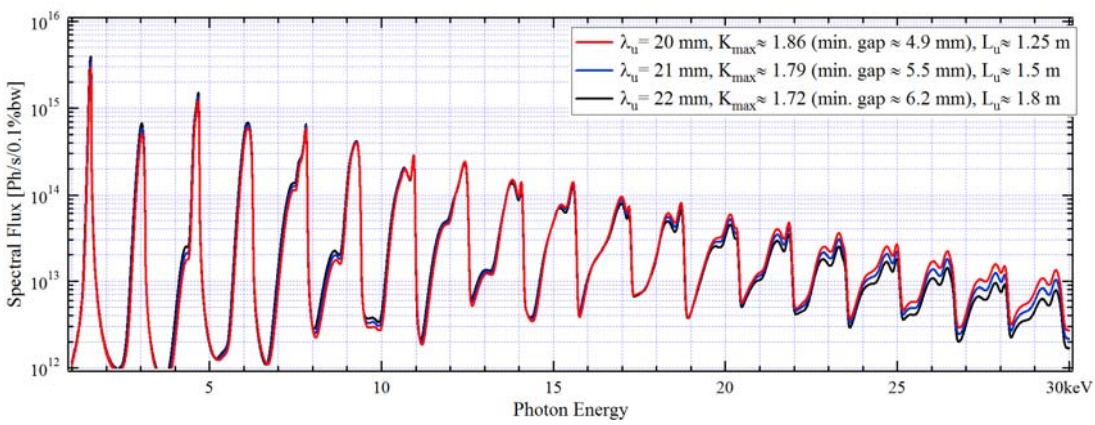

Figure 10. Spectral flux through an aperture with 0.1 x 0.1 mrad^2 size at minimal gap for three undulator setups as seen in the legend.

As the result of the above described calculations an in-vacuum undulator U21 has been chosen to work as the light source for the KB mirror branch. The parameters are listed in Table 3.

Table 3: Parameters in-vacuum undulator U21.

Undulator length	1.5 m
Period length	21 mm
Minimum gap	5.5 mm
Lowest energy in 3rd harmonic (E=3GeV)	4.65 keV
Maximum energy	28 keV
K-Value	1.79

ZP Branch

The ZP branch is dedicated to an energy range from E =2 keV up to E = 15 keV. When looking at the parameters of the standard undulators IVU 20, IVU 21, or IVU 22 and at the minimum allowable gap of 5.0 mm, it becomes clear that due to these limitations there will be an energy range between E = 4 keV and E = 5 keV, where no radiation can be delivered. From the viewpoint of scientific applications this cannot be accepted, therefore a solution has to be found to close this energy gap. Two ways to solve this problem are possible. The first solution would be to shorten the length of an undulator IVU 22 to 1.2 m. This would allow the minimum gap to be reduced without deteriorating the electron beam. Due to the resulting higher magnetic field strength the full desired energy range would be covered. However, due to the shorter length, the overall performance in terms of photon flux will be poorer. The other solution would be to insert a cryo-cooled IVU 22 undulator. Due to cryo-cooling a higher K-value would be achievable resulting in a full coverage of the desired energy range without hampering the electron beam even at the full length of 1.5 m.

2.3 Front End

A typical layout of a standard front end designed by NSLS-II can be seen in Figure 11. In principle, the components are comparable to the needs of the SRX beamline, however, due to the canted design several modifications are necessary. All elements have to be prepared for accommodating both beams from the two undulators. This is taken into account in the list of components that is found in chapter 2.7 of this report. The layout incorporating these constraints and special demands is work in progress.

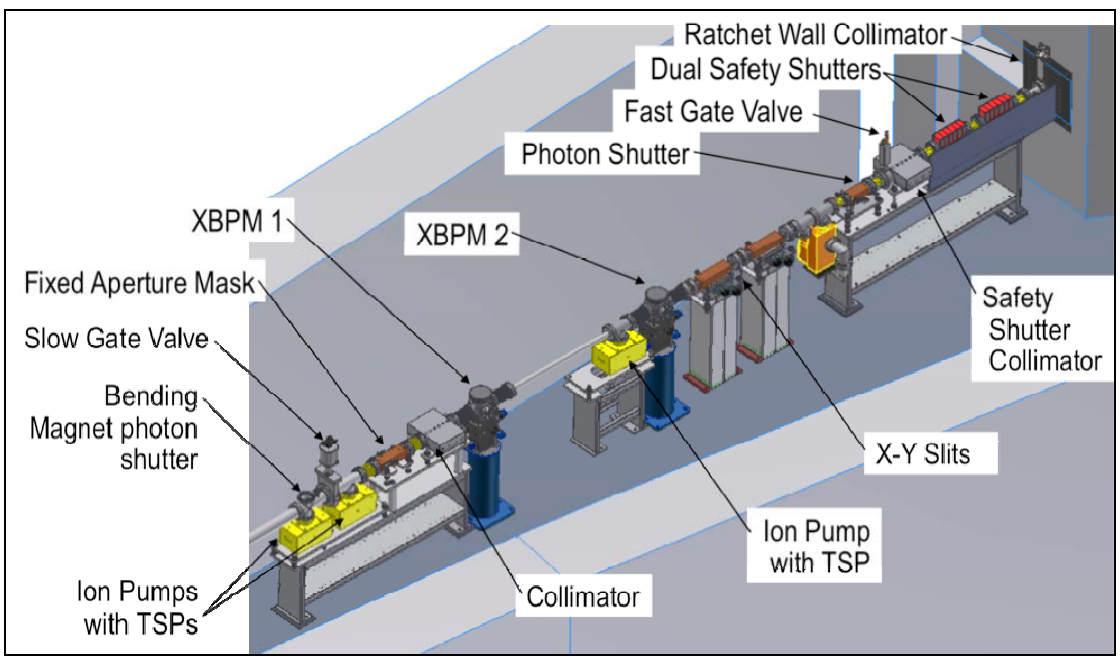

Figure 11. Layout of a standard front end of the NSLS-II SRX.

2.4 Optical Layout

The proposed optics plan is designed to provide state of the art x-rays, to accommodate a wide range of measurement needs and to maximize availability of beamtime for the earth, environmental and life science user communities. By canting two undulators and separating the optics into a lower energy line using zone plate (ZP) optics and a higher energy line with a Kirkpatrick-Beaz (KB) mirror system an extraordinary amount of new science will be accomplished by a very active and large user community. The complementary nature of the two lines together with a sector staffed with scientists possessing a wide range of synchrotron expertise will allow fluid and agile investigation of complex problems that often require a multitude of measurement types to solve.

In the following section the description of the optical layout starts in the front end and follows the beam downstream branching in the FOE, describing the optics of each line separately. This optics plan is based on the source parameters inserted as Table 1 in this document.

2.4.1 Common Components

Figure 5 shows a schematic of the sector. Located in the straight section are two undulators canted by 2 mrad. The midpoint between these undulators is used as a zero point for the distance values described in the following text. The 2 mrad separation in the center line of each undulator beam provides sufficient space to place separate apertures around each beam even before they exit the shield wall. It is proposed that a front end aperture (FEA) acting as a power and conductance limiter be placed as close the storage ring as possible. Such an aperture should be adjustable in both horizontal and vertical position and width and will most likely consist of two apertures one that is fixed and large designed to stop most of the unwanted power followed by a motorized second aperture exposed to a power load of 300 watts or less. This FEA will save space by acting as a differential pump and significantly reducing the x-ray power that enters the FOE. The reduce power will improve optics stability, a critical design requirement for this beamline. Once the beams enter the FOE front wall at 25.5 m they will pass through a pair of white beam filter (WBF) racks at 26 m that can be used to filter out low energy power as well as aid in diagnosing the performance of the beamline optics. Following the white beam filters will be a pair of horizontal and vertical white beam slits (WBS) that will further define the beam and be used as the beamlines primary storage ring diagnostic by configuring them as a pinhole camera and white beam profiler. Following the WBS the optics for the ZP line and KB line separate.

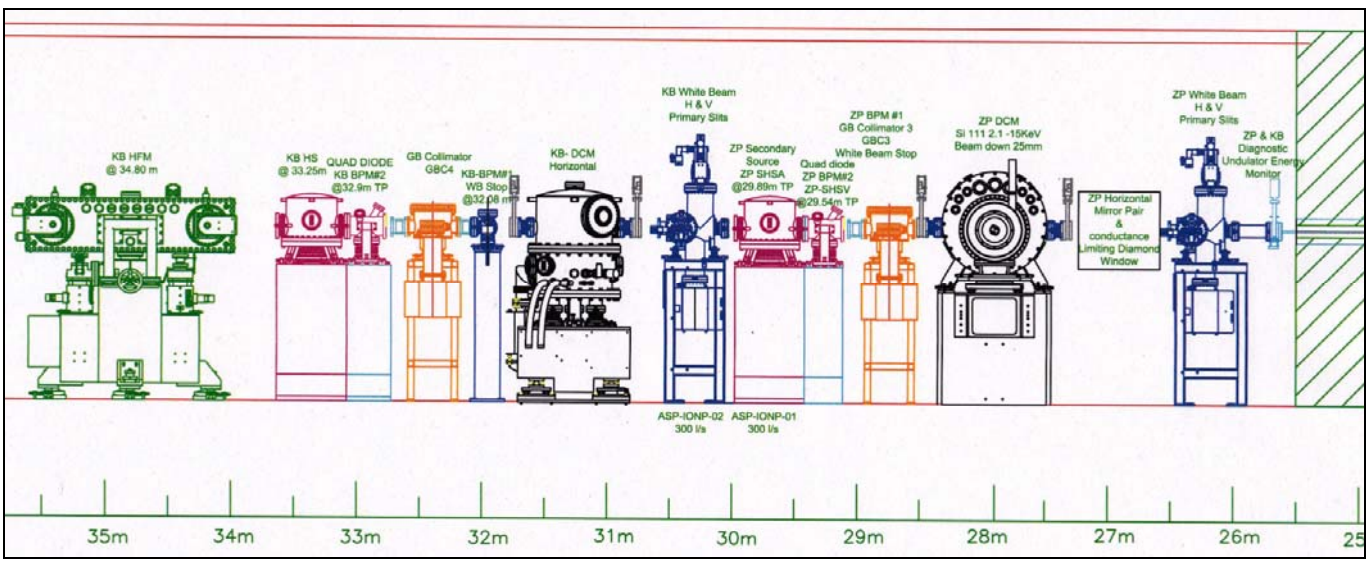

Figure 12. Layout of the beamline components in the First Optical Enclosure (FOE). For a detailed description of the components see chapter 2.7.

2.4.2 KB Branch

Figures 31 and 32 illustrate the horizontal and vertical optics layout for the KB line respectively. The KB line FEA will allow 4 sigma of the source to be delivered to a LN_2 cooled Si (111) / (311) double crystal monochromator. The monochromator, located at 34.8 m, will bounce the beam inboard 25 mm over an energy range of E = 4 keV to E = 25 keV. This monochromator is a horizontally deflecting design. The advantage is of course the larger separation of the two branches of this beamline. This happens to the expense of a potentially somewhat lower spectral resolution of this monochromator when using the full beam, as the horizontal divergence of the incoming beam is larger than the vertical. Accepting a trade-off in photon flux this can be compensated for by closing the slits and so not having to deal with the full divergence. The monochromatic beam illuminates a 1.2 m long water cooled Si horizontal focusing mirror (HFM) half coated with rhodium and operating at a fixed incident angle of 2.5 mrad. The HFM is located at 34.8 m and deflects the beam inboard forming a secondary horizontal focus at 56.5 m with a

demagnification of 1.85. The KB line beam passes by the experimental table of the ZP line endstation approximate 0.5 m inboard contained in a narrow profile shielded transport pipe.

Located at the upstream wall in the KB line endstation is a secondary horizontal source aperture (SHSA). The SHSA will be identical to the one used on the ZP line with a BPM used to stabilize the secondary horizontal source by controlling the HFM pitch. Inserted into Figure 31 at the secondary horizontal source location is a scatter plot of the 37 μm FWHM focal spot created by the HFM, also inserted is a scatter plot of the beam transmitted through a SHSA set to 2.7 μm horizontal width. The secondary horizontal focus is re-imaged by a 100 mm long horizontal KB mirror with a focal length of 80 mm, demagnification of 35 and a divergence of 3 mrad. Inserted into Figure 31 at the final focus location are two scatter plots, one showing the final horizontal focus of 1099 nm FWHM with the SHSA full open (transmitting 95% of the source) and the other showing a final focus of 71 nm FWHM with the SHSA set to 2.7 μm width (transmitting 7%).

The vertical focusing optics plan exploits the low vertical divergence of the source by utilizing a single 280 mm long vertical focusing mirror at 56.23 m (see Figure 32). This mirror is capable of collecting nearly the full vertical source divergence and focusing it 270 mm away to a focal spot of 70 nm with a divergence of 2.5 mrad. Figure 33 shows scatter plots and histograms for the SHSA full open (left panel) and set to 2.7 μm (right panel). By adjusting the SHSA the size of the final horizontal source can be tuned to best match the requirements of the experiment, allowing a trade off of flux for beam size. The vertical source can be made larger by defocusing the mirror using the bender. The ray traces were performed using ideal elliptical mirrors and in order to achieve the 100 x 100 nm goal the total RMS slope errors needs to be under 0.2 μrad. A total RMS slope error this low will require advances in mirror manufacturing and figuring technology but giving the recent progress in reflective x-ray optics it can be expected that mirrors of this quality will be available in the next five years.

Using a source brightness at 0.1 nm of $7x10^{20}$ phot/sec/0.1%bw/mm^2/$mrad^2$, a 0.4 correction for a 1.2 m long device, a triple mirror reflection efficiency of 70%, and an open SHSA collecting 95% of the full source the total flux delivered to 1000 x 100 nm (HxV) FWHM focus is 7 x 10^{13} phot/sec and with the SHSA set to 2.7 μm collecting 7% of the full source the flux delivered to a 100 x 100 nm focus is 5 x 10^{12} phot/sec.

2.4.3 ZP Branch

The goal of the FOE optics for the ZP line is to provide a stable coherent source to illuminate a zone plate located on the endstation optical table. The goal of the ZP line is to produce a focal spot that is 30 nm with maximal intensity. The ZP line should be able to utilize a zone plate with an outer zone width ΔR_n = 25nm and a diameter D = 330 μm under optimum conditions. Working at a wavelength of λ = 0.1 nm the focal distance of such a zone plate is f = 83 mm. A zone plate with these parameters is not readily available but given the numerous development efforts underway on zone plates and other nano-focusing optics, it is anticipated that optics with this kind of capability will be available in the next five years. Promisingly, it has been shown recently (published by Y.-T. Chen et al. in Nanotechnology in 2008) that gold zone plates for x-ray energies higher than E = 8 keV can be used for spatial resolutions below 30 nm.

For a nanoprobe beamline utilizing a zone plate as a focusing optic it is important to consider the coherent divergence of the source, given by $S'_{coh} = \lambda / 2S_{coh}$ where S_{coh} is the FWHM of the source. At a wavelength of λ = 0.1 nm the NSLS II source is within a factor of 2 of being fully coherent in the vertical direction whereas the horizontal source is more than 30 times less coherent then the vertical. If the full source size is used this astigmatism in the coherence would require astigmatic optics that are incompatible with a planar, radial symmetric focusing lens such as a zone plate. Figure 34 in chapter 2.6.2 illustrates the case of using the full horizontal and vertical source size showing a ray trace at 50 m – a typical final optic focusing location. The intersection of the horizontal and the vertical red lines (Figure 34 a) mark the coherent area of the un-apertured source. Figure 34 b shows all the incoherent rays and Figure 34 c shows that a 37 x 329 μm (H x V) aperture would be required at the optic for coherent illumination and that such an aperture would transmit 0.7% of the full undulator source. Though this is incompatible with a ZP lens it may be compatible with crossed linear lenses such as Multilayer Laue Lenses

(MLL) and kinoform lenses, both of which are candidate lenses for creating focal spot sizes down to 1 nm and which are subject of extensive development efforts.

The typical approach to lifting the astigmatism in coherence is to place a pinhole aperture as close to the source as possible. For the NSLS II only the horizontal beam size would need to be reduced by such an aperture. Figure 35 in chapter 2.6.2 illustrates an optics layout that provides nearly symmetric coherent illumination for an optic located at 50 m. In this case a 6 x 96 μm (H x V) front end aperture (FEA) is located at 14.5 m. Such an aperture will produce a coherent horizontal divergence of 9.3 μrad and allows the full coherent vertical divergence to pass. The pair of scatter plots inserted at 14.5 m in the Figure 35 shows the incoherent rays that would be lost and coherent rays that pass through the aperture. The inserted scatter plot at 50 m shows that 0.4% of the total undulator source is available to coherently illuminate a zone plate lens with a diameter of D = 330 μm. Such a zone plate would then focus the beam 83 mm away to a spot size of 30 nm with a divergence of 4 mrad. Figure 36 shows a scatter plot along with the horizontal and vertical histograms of the source at the zone plate location.

The use of a small horizontal FEA (or one as close to the source as the storage ring and beamline optics allow) is often used on zone plate beamlines. An aperture this close also has the advantage of significantly reducing the power passed to the remaining optics.The disadvantage of this aperture is the significant technical challenge of designing a small and stable aperture subjected to such high power loads, as well as that it is relative inaccessible and the likelihood that it will need to be moved further downstream due to front end design constraints. As an alternative approach and one that works well in our canted beamline design is to use a horizontal mirror pair (HMP) as close as possible to the shield wall in the FOE. The HMP will both, deflect the beam horizontally creating beam separation at the endstation and form a secondary horizontal source (SHS) that can be manipulated by a secondary horizontal source aperture (SHSA). Figure 33 in chapter 2.6.2 illustrates this arrangement showing an FEA that is now much larger (60 x 96 μm) and only acting as a power limiter and differential pump (its exact location is also now flexible).

The HMP would be located at 28.8 m and focuses the horizontal source with a demagnification of 9 at 32 m. The HMP can be compact since the coherent horizontal divergence is low (4.1 μrad), requiring only an optical aperture (OA) with a diameter of 120 μm. The mirrors will be water cooled silicon, each half coated with rhodium and operating at a fixed 4 mrad incident angle for a total horizontal deflection of 16 mrad. The second mirror will have a dynamic bender that will correct for the thermal bump on the first mirror and focus the beam to approximately 7 μm FWHM at the SHSA. Located after the HMP and before the SHSA will be an indirectly LN_2 cooled Si (111) double crystal monochromator that bounces the beam down by 25 mm with an energy range of E = 2 keV to E = 15 keV. In this arrangement the SHSA will see no power load, eliminating the thermal stability concerns of locating such an aperture in the front end.

The SHSA will be an ultra stable horizontally adjustable aperture with an integrated beam position monitor (BPM) utilizing active feedback of the HMP deflection angle to produce a stable, small coherent horizontal source with approx. 3 μm FWHM for the zone plate located at 50 m. The insert in Figure 33 at the SHS location is scatter plot showing the full focus of the HMP of 6.6 μm FWHM and a scatter plot with the SHSA set to 2.7 μm. With the SHSA set to 2.7 μm the coherent horizontal divergence of this source is 19 μrad. This secondary source diverges to 330 μm at the zone plate located at 50 m (18 m downstream form the SHSA) thus symmetrically illuminating the final focusing optic (see inserted scatter plot at 50 m in Figure 35). Figure 34 shows an evenly illuminated 330 μm aperture at 50 m that transmits 0.8% of the full source. The experimental table mounted zone plate is expected to focus the beam to a 30 nm spot. Using a source brightness at 0.1 nm of $7x10^{20}$ phot/sec/0.1%bw/mm^2/$mrad^2$, a 0.4 correction for a 1.2 m long device, a double mirror reflection efficiency of 80%, a zone plate efficiency of 10%, together with the 0.8% of the full source results in a total flux delivered to the sample of $7x10^9$ phot/sec. One the main benefits of this optics plan for the ZP line is its flexibility in accommodating future developments in nano-focusing optics while at the same time allowing the specification and procurement of major beamline components.

2.5 High Heatload Optics

To maintain the stability of the focused beam and to ensure that the energy resolution of the SRX-KB monochromator is not significantly degraded for spectroscopic studies, we carefully evaluated the positioning of possible white beam components in the first optical enclosure so as to minimize errors resultant from heating. Two arrangements are proposed for the horizontally focusing mirror (HFM) design, a monochromatic beam mirror located downstream of the double crystal monochromator (DCM), and a mirror capable of accepting the white beam. It turns out, that the first crystal of the DCM will be better able to master the heat load stemming from the undulator than the horizontally focusing mirror, at the same time keeping the optical performance of the beamline in its desired limits. Therefore, solution II will be pursued further on. Details of the calculations and the results leading to this conclusion will follow in this chapter.

2.5.1 Horizontally Focusing Mirror

The mirror has a total length of 1390mm, width 50mm and depth 50mm, with an optical area of 1200mm. The white beam option includes symmetric channels cut into the side faces along the length of the mirror, which are used for liquid gallium cooling. Both mirror options have two reflective stripes (rhodium & bare silicon) covering the length of the optical face of the mirror. Figure 13 shows the calculated reflectivity of the rhodium and silicon stripes at an incidence angle of 2.5mrad. For low energy reflection, silicon is shown to give high reflectivity and suppression of higher order harmonics. The rhodium stripe is used at the higher energies to maintain mirror reflectivity. The latter might be the option used almost all the time, as the desired energy range is fully covered with high reflectivity.

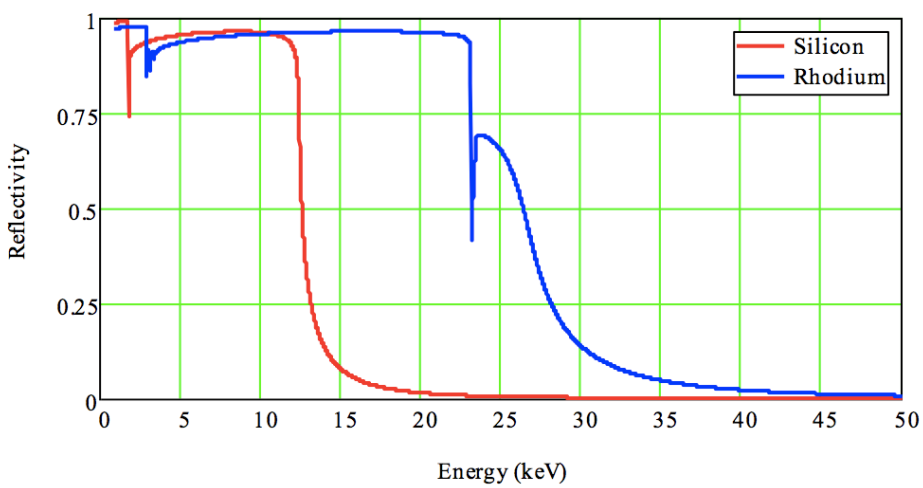

Figure 13. Reflectivity of silicon- or rhodium-coated mirror surfaces as a function of incident x-ray energy.

Based on the source, beam and undulator parameters the source spectral power distributions for the bare silicon and rhodium stripes are shown in Figure 14 and Figure 15 respectively. The transmitted spectral power distribution for each stripe is superimposed with the source distribution profile. The transmitted distribution is calculated by multiplying the source spectral distribution with the coating absorption characteristic (Figure 13). The sum of transmitted power at each energy is then divided by the sum of the source power at each energy to give the percentage transmission from the mirror. Relative to the source distribution at a grazing angle of 2.5 mrad, the power absorption for the bare silicon stripe has been calculated at 56.0%, while the rhodium stripe has been calculated at 18.4%.

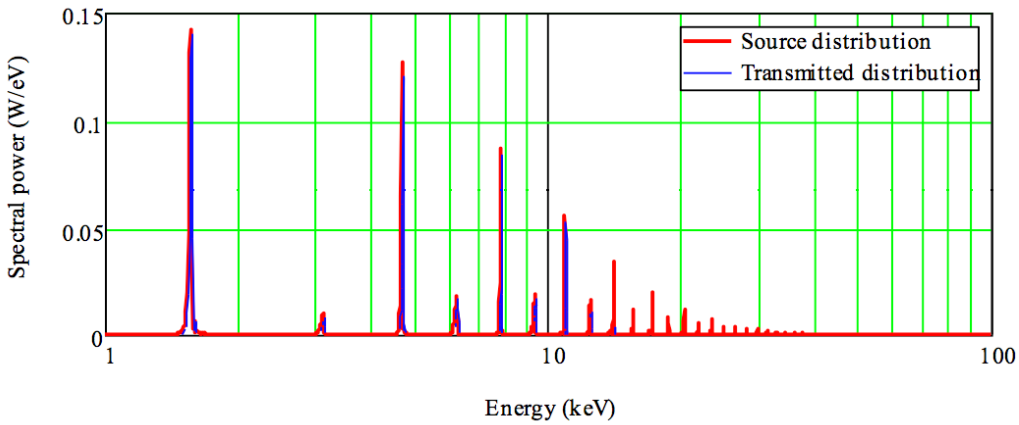

Figure 14. Spectral power absorption distribution for a bare silicon stripe.

The mirror is a super polished flat cut silicon mirror to horizontally collimate the beam using differential bending to figure the mirror to an approximation of the ideal collimating shape. To achieve this, two independent moments are applied to either end of the mirror producing a linear moment distribution along the mirror length. Although a uniform radius of curvature can readily be achieved with the two-moment bender, a key advantage in offering differential moment is that even a small deviation from ideal can be reduced or eliminated as desired. The principle of the bending mechanism is shown schematically in Figure 16. Applying the bending forces to the mirrors through bending holes below the surface allows any distortions resulting from contact strain to dissipate before reaching the optical surface.

The tangent point of the monochromatic beam mirror is that given in NSLS-II documentation. For the purposes of this study the white beam mirror option is treated as the first optical component, with the tangent point taken as 31.7m (that of the DCM). The mirror operates at a fixed incident angle of 2.5mrad.

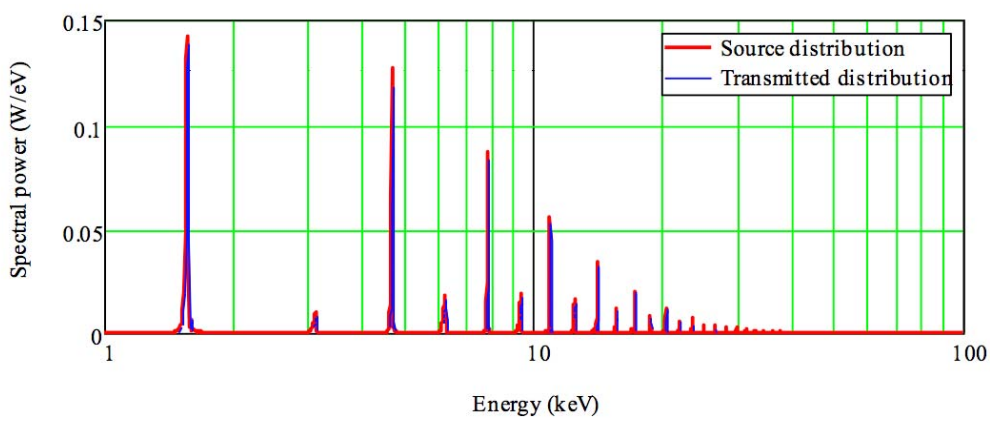

Figure 15. Spectral power absorption distribution for the rhodium stripe.

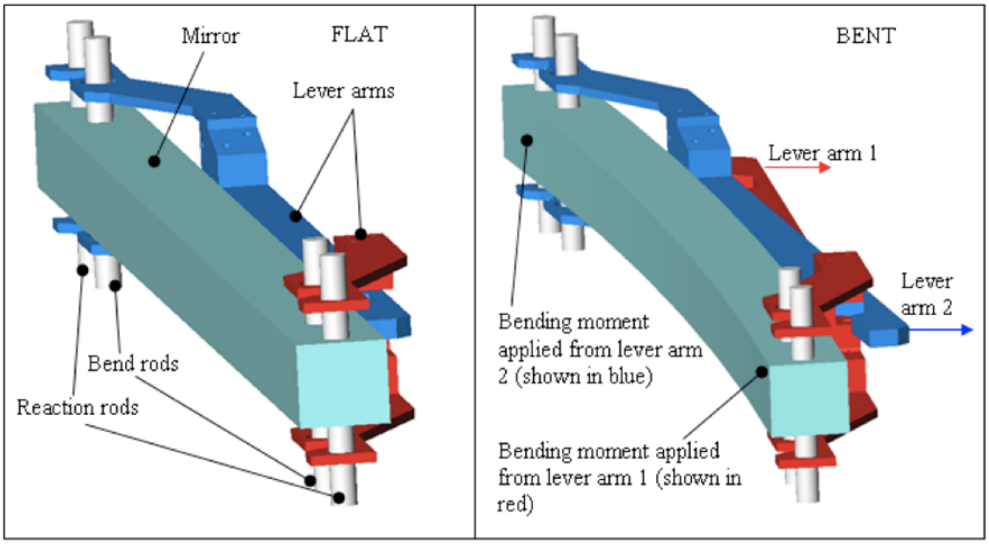

Figure 16. Bending principle suggested for the horizontally focusing mirror.

For the white beam mirror option, a finite element analysis model of the mirror is run to determine the mirror displacement due to the thermal heat load. The beam size incident on the white beam mirror has been set at 94.6µrad horizontally by 100µrad vertically. Based on this size, the transmitted power through the slits and incident on the mirror is calculated at 248.7W. The 'worst case' mirror absorption has been calculated at 56% when using the bare silicon reflective stripe.

To apply the thermal load, an area representative of the beam footprint is projected onto the optical surface. The undulator angular power density distribution is fitted with a Gaussian function, which is projected onto the optical surface at the appropriate incident angle. An optically active length of 1200 mm corresponds to a beam acceptance of 94.6µrad (horizontally) x 100µrad (vertically). The total heat load incident upon the crystal is 139.3W, with an on-axis power density of 15.6kW/mrad^2.

Convective cooling is applied through the top gallium groove, with an applied heat transfer coefficient of 1W/cm^2/ºC. Calculations indicate that a heat transfer coefficient of 1.5W/cm^2/ºC would be achievable inside the coolant pipe with a diameter of 6 mm bore. The heat transfer coefficient value applied inside the gallium grooves is lowered to account for the larger wetted area of the grooves relative to the internal area of the coolant pipe.

The results from the thermal model (shown in Figure 17) are then loaded into a structural model, with appropriate constraints applied to the mirror to allow free expansion. Material properties for silicon are taken from the Material Property Database program.

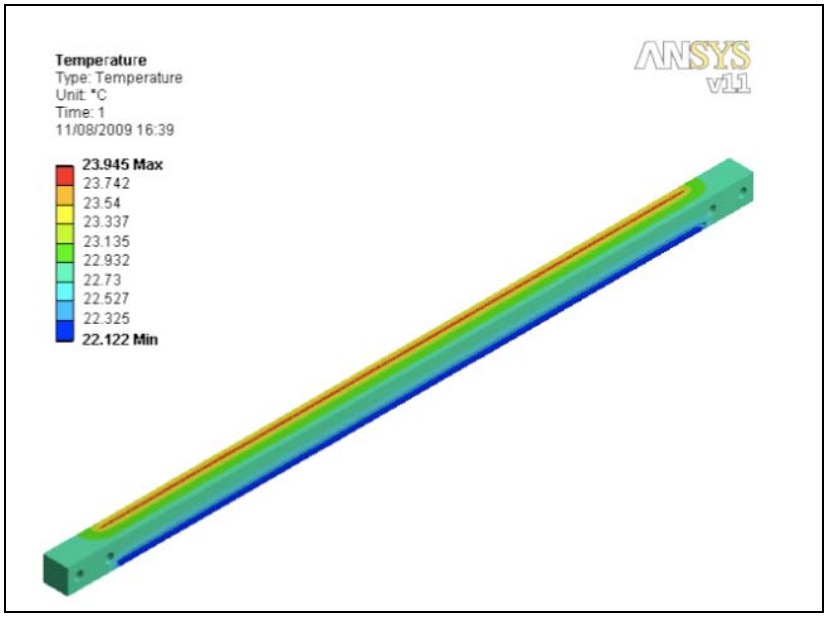

Figure 17. Temperature distribution on a mirror in white beam.

The focal length, the incidence angle and the optical length of the mirror define the ideal mirror bend profile. To induce the bend and achieve the required central deflection, which is determined from the ideal bend profile, loads are applied at either end of the mirror through the bending mechanism. For the monochromatic beam mirror a load of 113.9 N applied at each end is calculated to give the required deflection at the mid-span location. Figure 18 superimposes the calculated mirror bend profile using this bending load with the ideal profile.

For the white beam mirror option, the effects of the thermal heat load of the white beam must also be considered. In this case, the applied bending load is calculated to compensate for the effect of the thermal bend to give the correct mirror profile. A bending load of 131.7 N is required by the white beam mirror to give the correct profile. The bend profiles for the white beam mirror are shown in Figure 19.

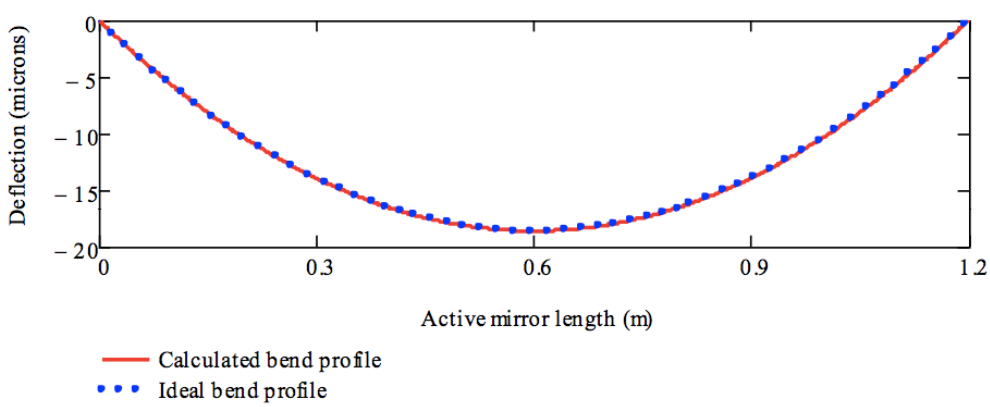

Figure 18. Comparison of the calculated and the ideal mirror bend profiles for a mirror in monochromatic beam downstream of the monochromator.

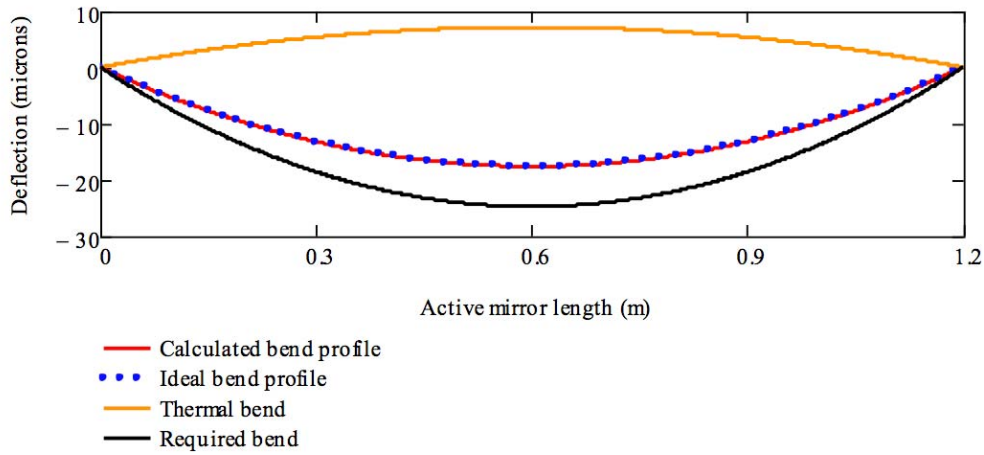

Figure 19. Comparison of the required, the calculated, the ideal, and the thermally induced mirror bend profiles for a mirror in white beam.

The bending loads determined from the ideal bend profile are applied to the finite element analysis model of the mirror (along with the thermal load in the case of the white beam mirror) to determine the actual bend profile.

The residual (uncorrectable) slope error is defined as the difference between the actual mirror slope profile (given by differentiation of the bend profile determined by the finite element analysis model) and the ideal slope profile. The residual slope errors for the monochromatic and white beam mirrors, calculated over the optically active length, are shown in Figure 20 and Figure 21 respectively. A root mean square (RMS) slope error of 0.076μrad is calculated for the monochromatic beam mirror, and 0.599μrad for the white beam mirror.

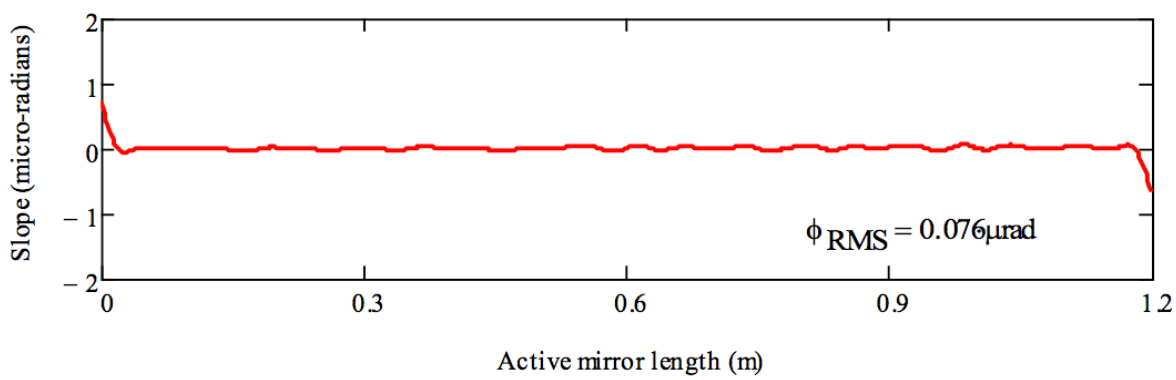

Figure 20. Residual slope error along the length of the mirror for monochromatic beam downstream of the monochromator.

A summary of the key criteria of the mirrors is given in Table 4. The monochromatic beam mirror design, gives negligible residual slope errors. The white beam mirror option on the other side gives slope errors, which would affect the performance of the SRX beamline.

Table 4. Key criteria for Horizontally Focusing Mirror Options

Description		Focussing mirror, reflecting horizontally
Substrate material		Single crystal silicon
Substrate dimensions		1390mm long x 50mm wide x 50mm deep
Reflective coatings		Silicon (<12keV), Rhodium (10-28keV)
Optically active length		1200mm
Incidence angle	θ	2.5mrad
Monochromatic beam mirror		
Focal lengths	F_1	33.8m
	F_2	18.8m
Beam acceptance		86μrad (h) x 100μrad (v)
Radius of curvature	$R = \frac{2}{\left(\frac{\sin(\theta)}{F_1} + \frac{\sin(\theta)}{F_2}\right)}$	9.66km
Calculated bending load		113.9N
RMS slope error		0.076μrad
Calculated bending stress	$\sigma = y \cdot \frac{E}{R}$	0.34MPa
White beam mirror option		
Focal lengths	F_1	30.7m
	F_2	21.9m
Beam acceptance		94.6μrad (h) x 100μrad (v)
Radius of curvature	$R = \frac{2}{\left(\frac{\sin(\theta)}{F_1} + \frac{\sin(\theta)}{F_2}\right)}$	10.23km
	Calculated bending load	131.7N
	RMS slope error	0.599μrad
Calculated bending stress	$\sigma = y \cdot \frac{E}{R}$	0.32MPa

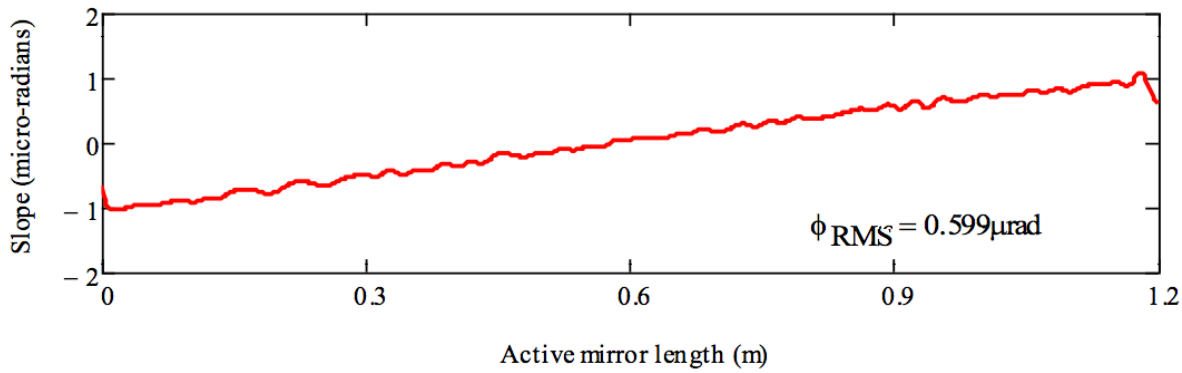

Figure 21. Residual slope error along the length of the mirror for white beam.

2.5.2 Double Crystal Monochromator

Heat load calculations have been made for the first crystal of the double crystal monochromator to evaluate whether it will be possible to have the monochromator as a first optical element in front of the horizontally focusing mirror without harming the spectral and optical performance of the beamline.

An indirect cryogenic cooling arrangement is proposed for the crystal design. The design of the crystal holder is similar in principle to a design successfully implemented by the company IDT at the Australian Synchrotron, with the 1st crystal sandwiched between two cooled copper blocks. To improve vibrational stability, short lengths of copper braid will be used to connect the LN_2 coolant pipe to the copper blocks, mechanically decoupling the crystal from the cooling circuit. The design accommodates four crystals (Si (111), Si (311) and two multilayer crystals).

To provide good thermal contact, Indium foil is used between the sides of the silicon and copper blocks. The indium foil has a secondary benefit of absorbing the differential expansion between the copper blocks and silicon crystal and limits the resulting stress and strain transmitted to the optical surface of crystal.

To determine the crystal displacement due to the thermal heat load, an FEA model of the crystal was run. This chapter shows the finite element analysis results for the silicon crystal only.

Previous thermal analysis of monochromator crystals has shown that the primary design case for selecting the crystal design is generally fixed by the optical performance at the higher energies as a result of the narrower Rocking Curve widths. Figure 22 shows that the narrowest Rocking Curve width is 9.9μrad for Si (111) at E = 28 keV, and 3.8μrad for Si (311) at E = 28 keV. These high energies are used as the primary design case for finite element analysis modeling.

A secondary design case of Si (111) at E = 4.65 keV is also implemented in this study. This low energy configuration requires the largest Bragg angle, which gives the smallest beam footprint and therefore the highest incident power density.

The crystal size used for the finite element analysis model is similar to that used on the Australian synchrotron monochromator. The crystal has length 80 mm, width 30 mm and depth 30 mm.

The second crystal length and the beam offset determine the workable range for the Si (111) and Si (311) crystals. A beam offset of 25mm and a second crystal length of 180mm allows Si (111) to operate over the full energy range from E = 4.65 keV up to E = 28 keV.

Figure 22 shows that for the low energies Si (311) requires a very large Bragg angle, which limits the lowest energy accessible to Si (311). For a 25 mm beam offset, the minimum energy of Si (311) is E = 6.5 keV. This minimum can be lowered by increasing the beam offset value.

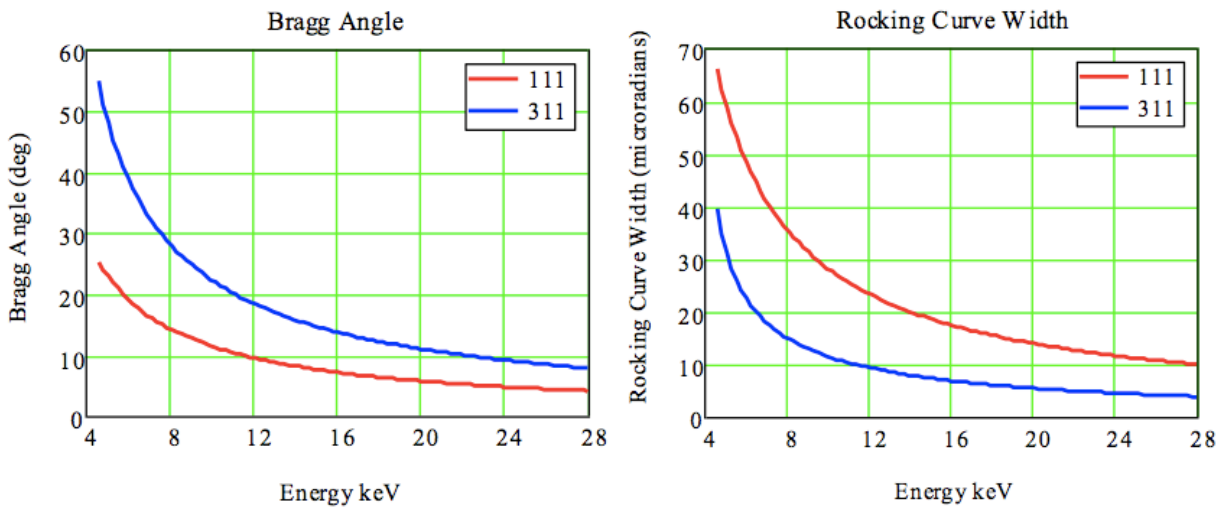

Figure 22. Bragg angle (left) and width of rocking curve (right) for Si (111) in red and Si (311) in blue.

To apply the thermal load, an area representative of the beam footprint is projected onto the optical surface. The undulator power density distribution is fitted with a Gaussian function, and this Gaussian is then projected onto the optical surface at the appropriate Bragg angle. For a beam acceptance of 100 µrad x 100 µrad, the total heat load incident upon the crystal is 263W, with an on-axis power density of 27.8kW/mrad^2.

Convective cooling is applied to the cooled contact area between the crystal and the copper heat exchangers. Based on a hydraulic diameter of 10mm and a LN_2 flow rate of 4litres/min, a heat transfer coefficient at the LN_2 heat sink of 2360W/m^{2}K is calculated using the Dittus-Boelter correlation. With the inclusion of thermal contact and conduction resistances, an effective heat transfer coefficient at the crystal contact of 1700W/m^{2}K is calculated by considering the entire cooling circuit, with the bulk temperature on the contact surface set to 80 K.

Material properties for silicon are taken from the Material Property Database program.

The results of the thermal model are loaded into a structural model, with restraints applied to simulate clamping and allow free expansion.

Figure 23 shows the temperature and displacement distribution for Si (111) at E = 28 keV, while Figure 24 shows the slope error profile of the crystal at this energy.

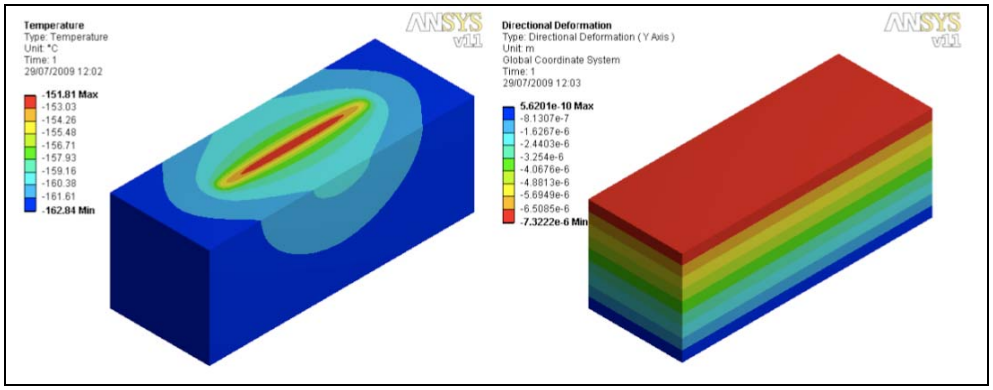

Figure 23. Spatial distribution of temperature (left) and deformation along the vertical axis (right) for Si (111) at E = 28 keV.

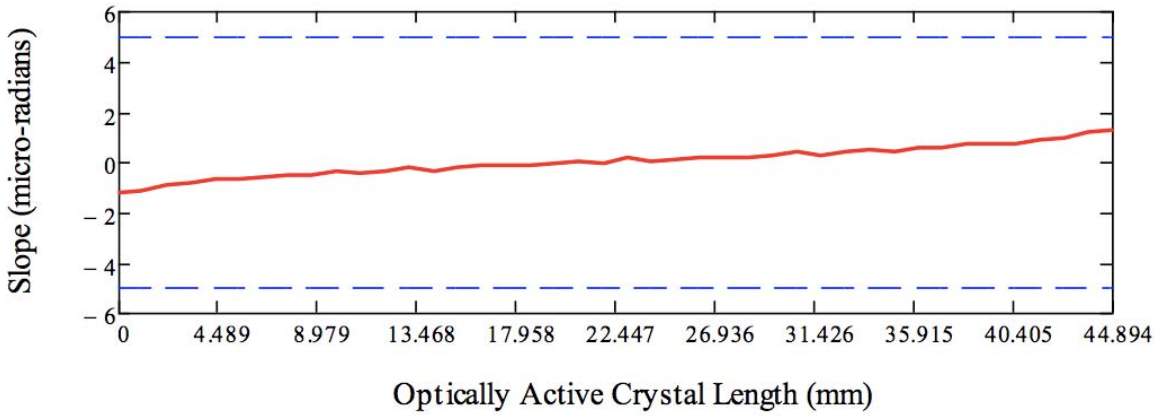

Figure 24. Tangential slope profile for Si(111) at E = 28 keV. The dashed blue lines show the rocking curve limits.

The case of Si (111) at E = 4.65 keV gives the highest incident power density. This energy has a large rocking curve width of 65.8 μrad. The results for this energy, given in Figures 25 and 26, show that the slope error is easily under the rocking curve limit at this energy.

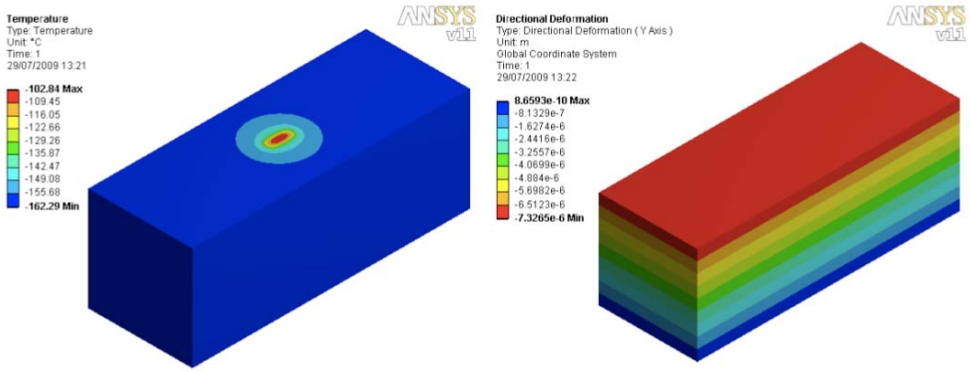

Figure 25. Spatial distribution of temperature (left) and deformation along the vertical axis (right) for Si (111) at E = 4.65 keV.

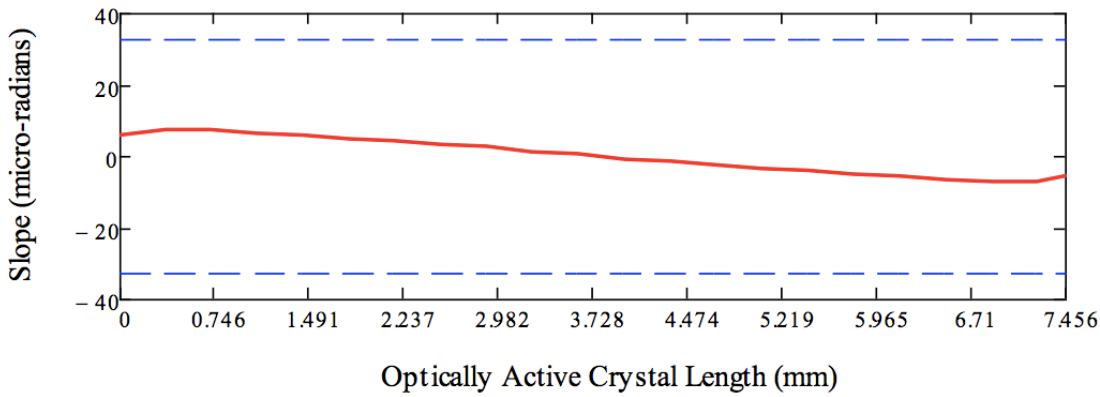

Figure 26. Tangential slope profile for Si (111) at E = 4.65 keV. Dashed blue lines show the rocking curve limits.

Figure 27 shows the temperature and displacement distribution for Si (311) at E = 28 keV, while Figure 28 shows the slope error profile of the crystal at this energy.

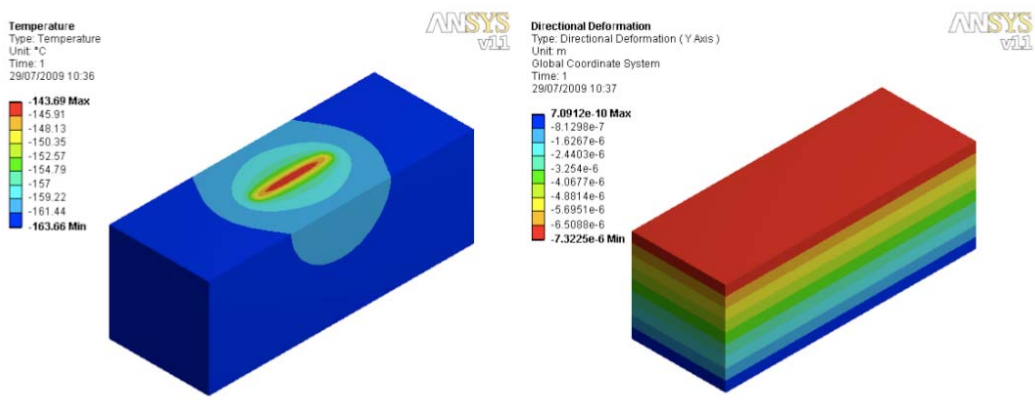

Figure 27. Spatial distribution of temperature (left) and deformation along the vertical axis (right) for Si (311) at E = 28 keV.

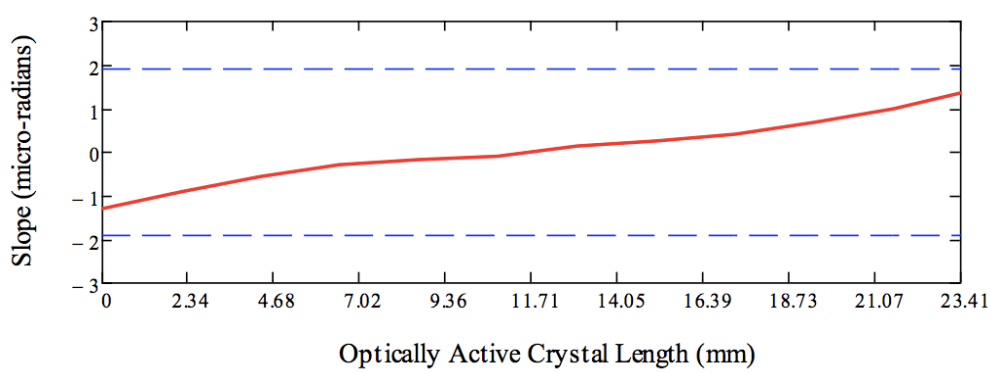

Figure 28. Tangential slope profile for Si (311) at E = 28 keV. The dashed blue lines show the rocking curve limits.

Figures 29 and 30 show the results for Si (311) at the lowest energy attainable with the 25mm beam offset design (E = 6.5 keV). The rocking curve width here is 20.1 µrad.

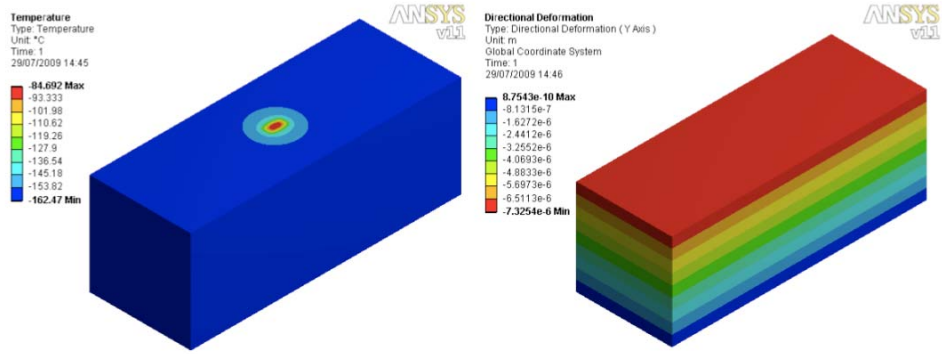

Figure 29. Spatial distribution of temperature (left) and deformation along the vertical axis (right) for Si (111) at E = 6.5 keV.

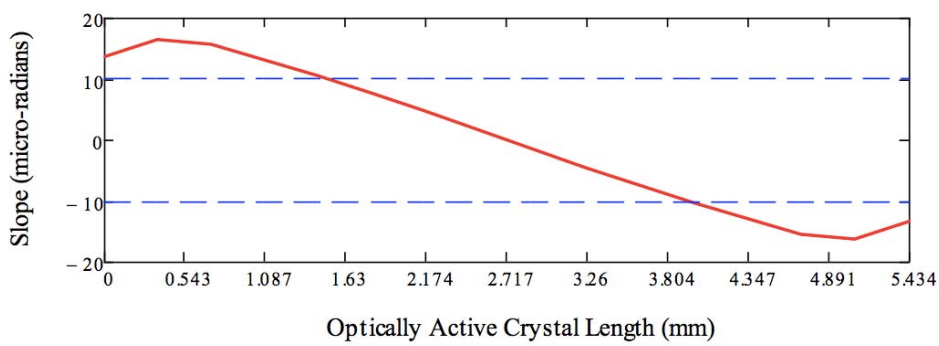

Figure 30. Tangential slope profile for Si (311) at E = 6.5 keV. Dashed blue lines show the rocking curve limits.

It is clear from these results that the slope error at this energy is larger than the rocking curve width. Figure 22 shows that the Bragg angle necessary to access this energy is much larger than that required for Si (111). A much larger Bragg angle gives a much higher incident power density. It is this high power density that will limit the lowest energy of Si (311) within the slope error requirements. The lowest energy of Si (311) giving both tangential and sagittal slopes under the rocking curve width is E = 8.5 keV.

Table 5, which also gives the sagittal slope errors for the energy configurations discussed, summarizes the findings of this study.

Table 5. Slope Error Summary.

Crystal Face	Energy	Rocking Curve Width	Tangential Slope Error	Sagittal Slope Error
Si(111)	4.65 keV	65.8 µrad	11.6 µrad	20.9 µrad
Si(111)	28 keV	9.9 µrad	2.5 µrad	1.0 µrad
Si(311)	6.5 keV	20.1 µrad	26.9 µrad	35.1 µrad
Si(311)	28 keV	3.8 µrad	2.6 µrad	0.8 µrad

The result of this study is that a braided cryo-cooled crystal of size 80 mm x 30 mm x 30 mm is feasible for the SRX beamline. The Si (111) crystal can operate over the full energy range from E = 4.65 keV to E = 28 keV within slope error requirements, while the Si (311) crystal operates over the reduced range of E = 8.5 keV to E = 28 keV.

2.6 Ray Tracing

2.6.1 KB Beamline

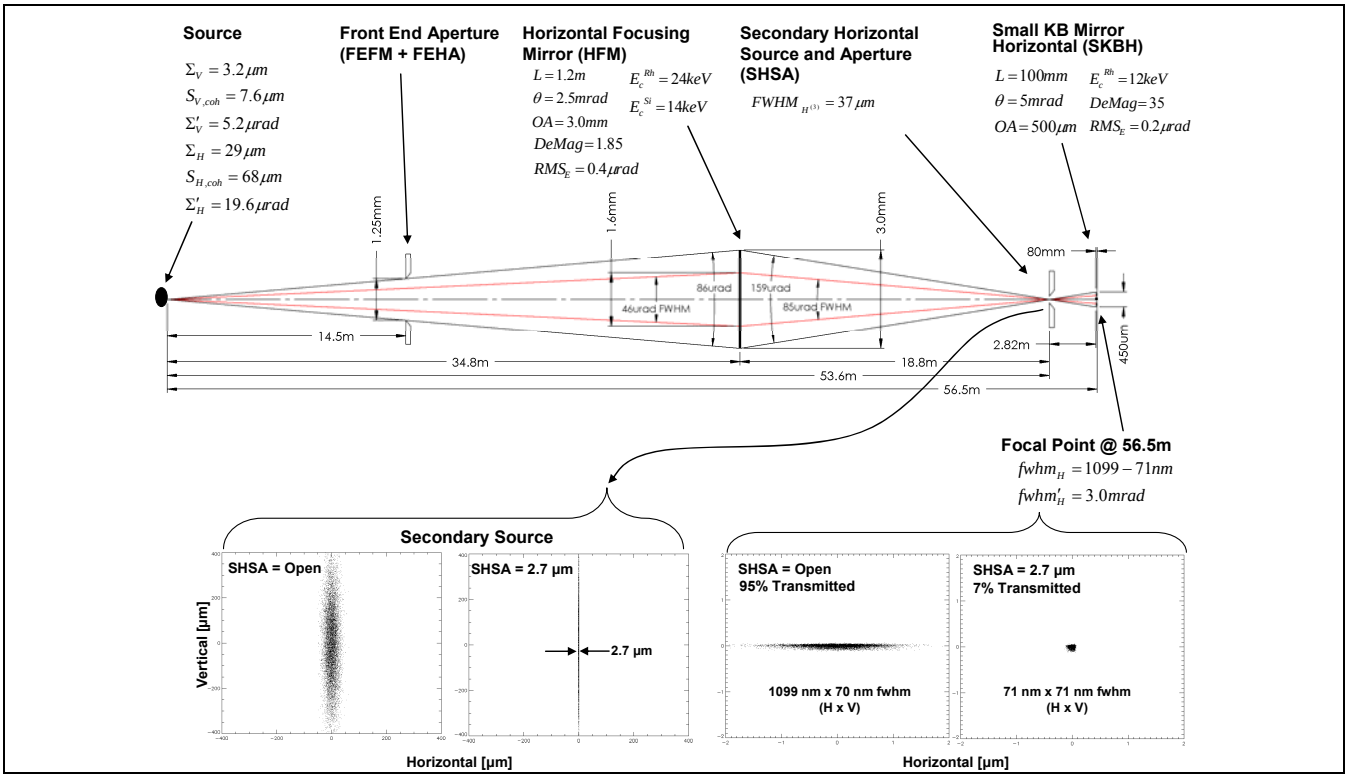

Figure 31. Horizontal optics layout and scatter plots for the KB beamline with a secondary horizontal source at 53.6 m, produced by a 1.2m long horizontal focusing mirror at 34.8 m at a fixed incidence angle of 2.5 mrad. Working distance ~ 30 mm

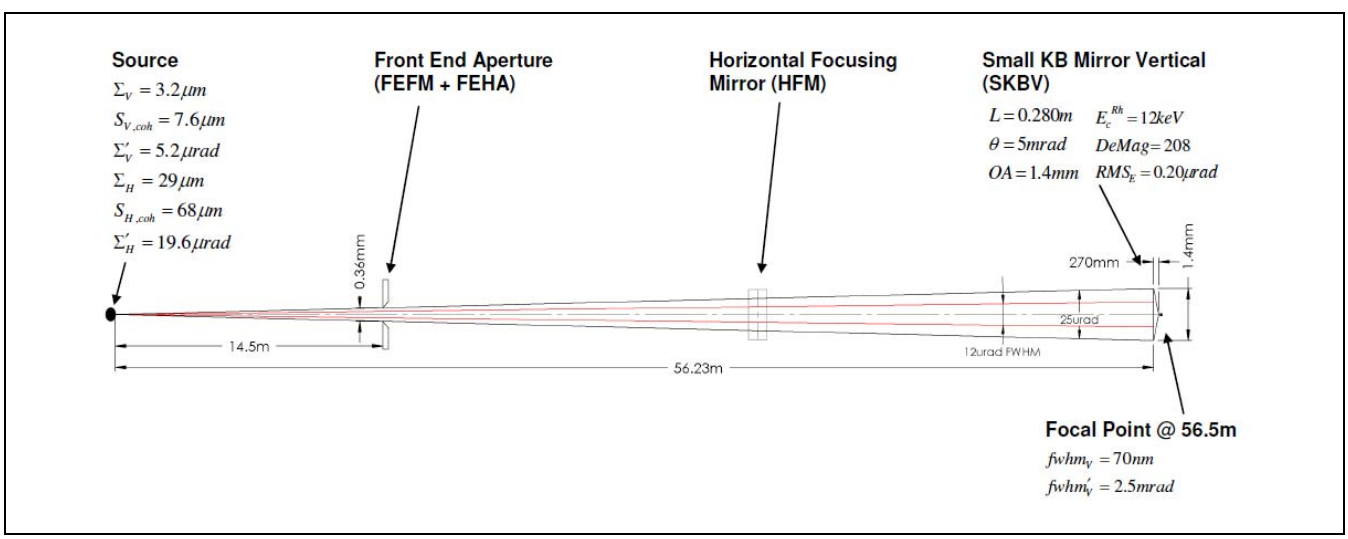

Figure 32. Vertical optics layout for the KB beamline showing a single 280 mm long vertical focusing at 56.23 m.

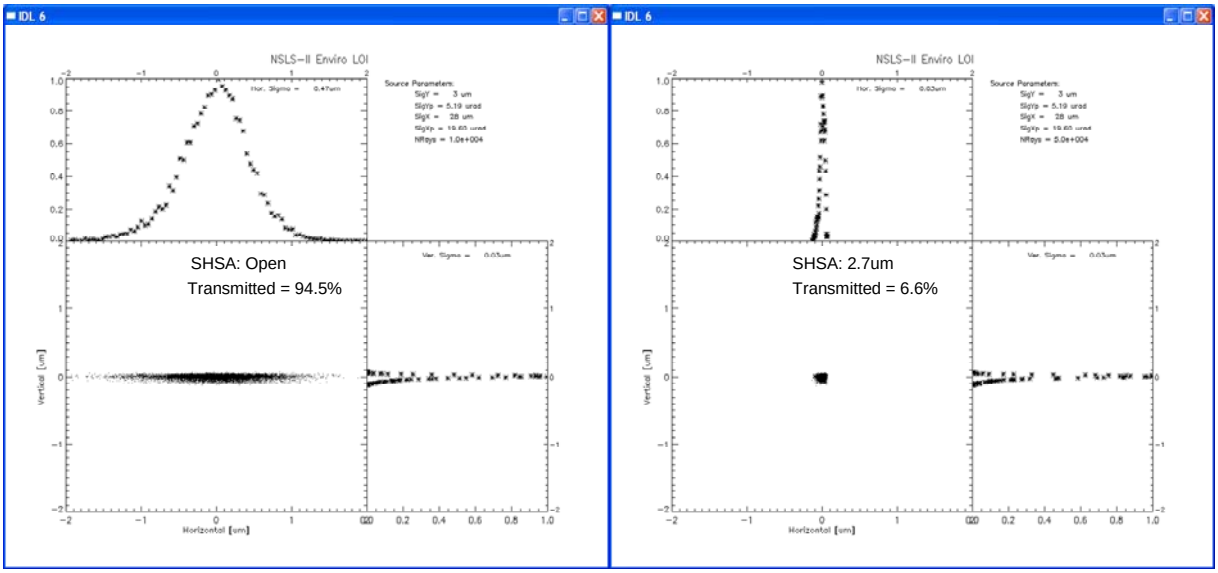

Figure 33. Scatter plots and horizontal and vertical histograms for the KB beamline showing two extreme settings of the secondary horizontal source aperture: full source (left panel) and set to 2.7 μm (right panel).

2.6.2 Zone Plate Beamline

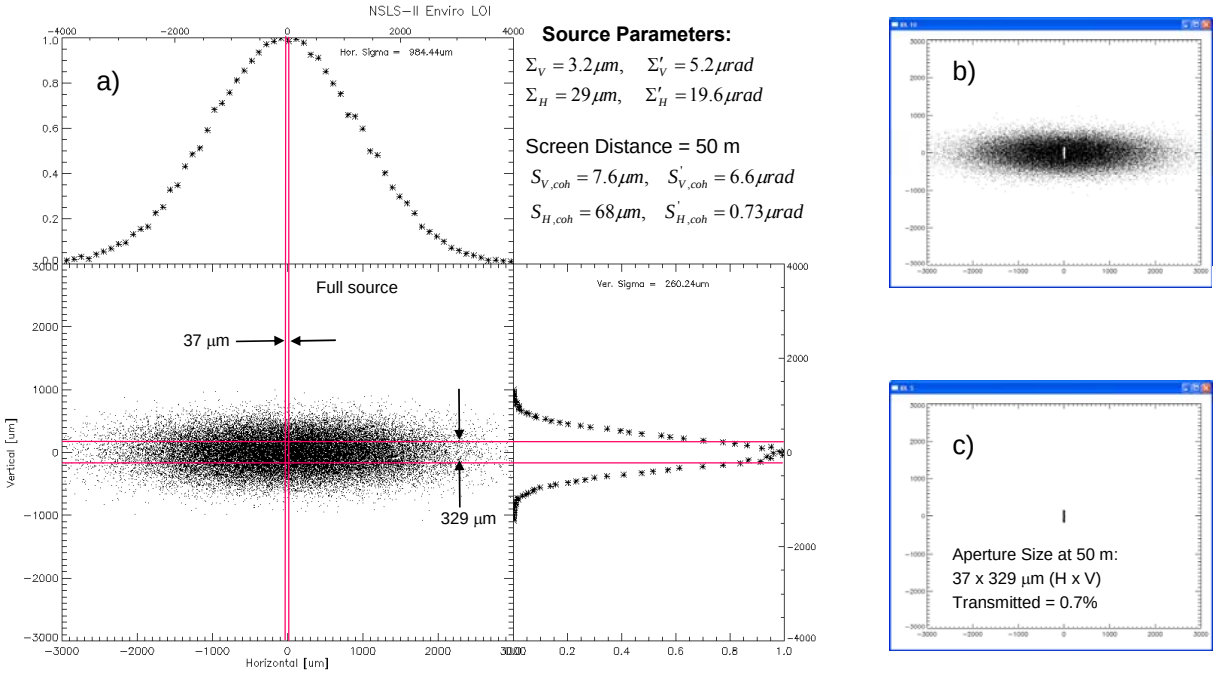

Figure 34. Scatter plot of a full source ray-trace at 50 m. a) Shows the horizontal and vertical histograms with the intersection of the red lines marking the coherent section of the source. b) Shows all the incoherent rays and c) the coherent rays into a 37 x 329 μm (H x V) aperture.

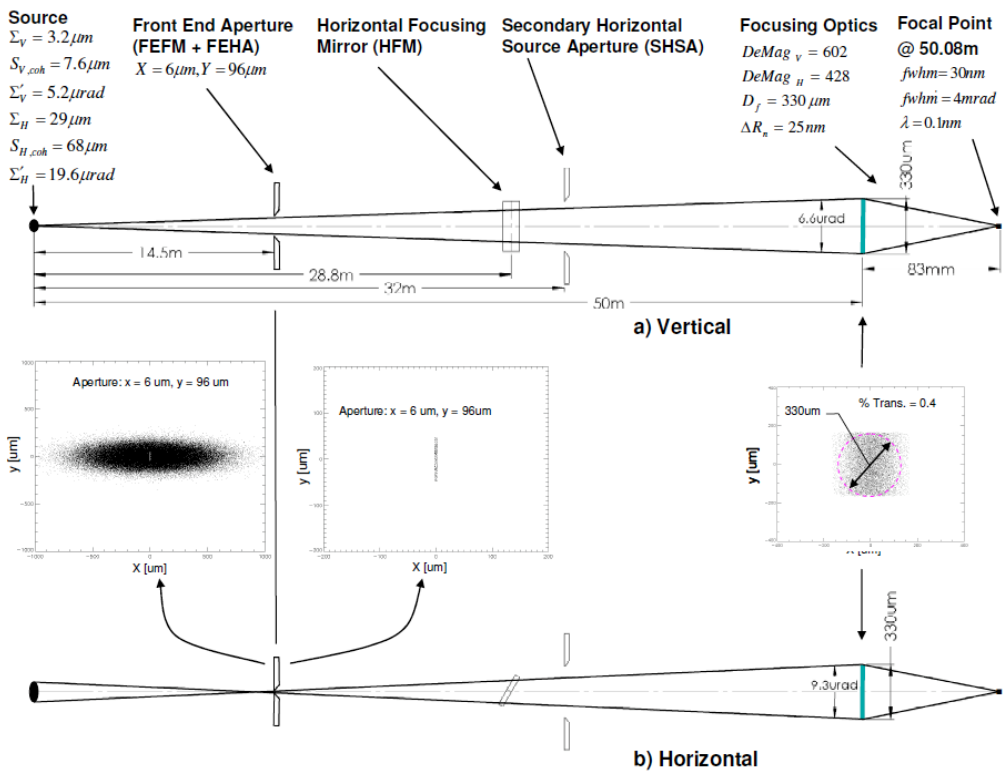

Figure 35. Optics layouts, ray trace and scatter plots for a ZP beamline utilizing a front end aperture to select the coherent fraction of the beam to illuminate a linear symmetric lens such as a zone plate.

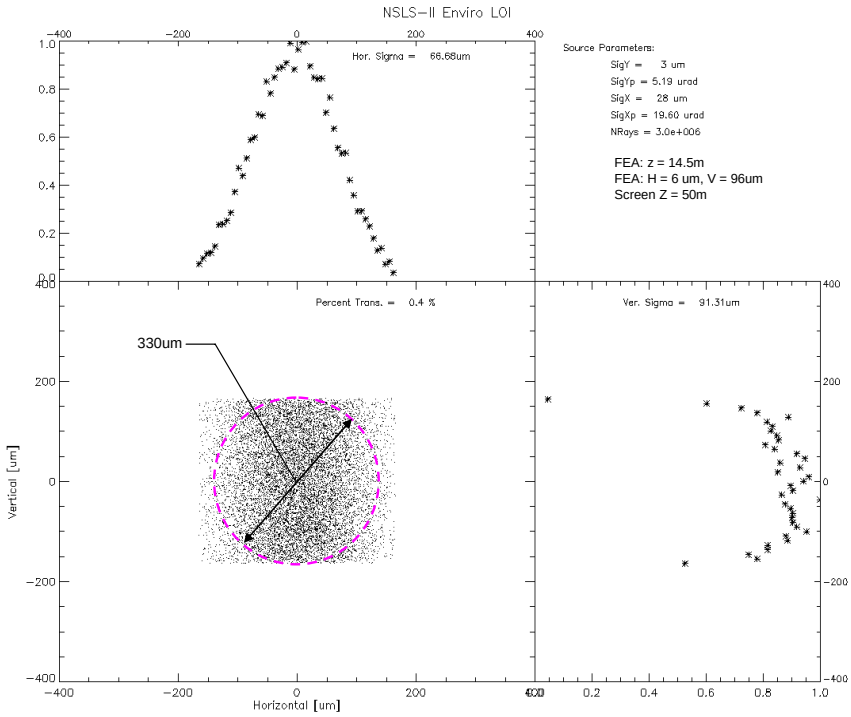

Figure 36. Scatter plot and horizontal and vertical histograms at the location of the zone plate at 50 m of the optics layout illustrated in Figure 35.

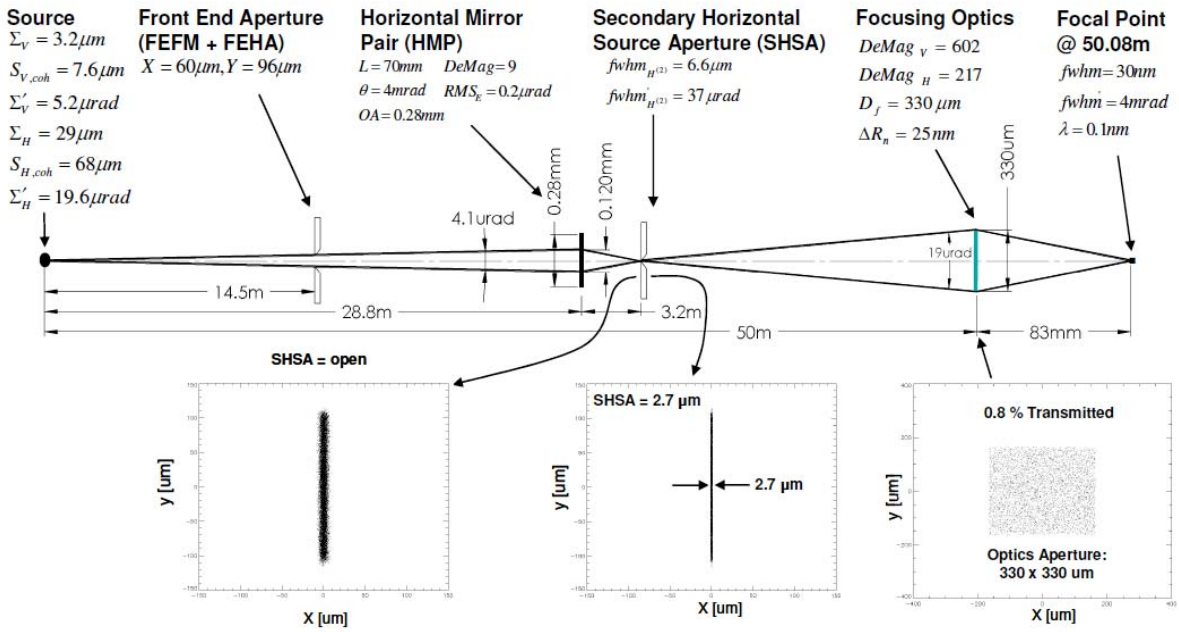

Figure 37. Horizontal optics layout and scatter plots for the ZP beamline with a secondary horizontal source point at 32 m produced by a horizontal focusing mirror.

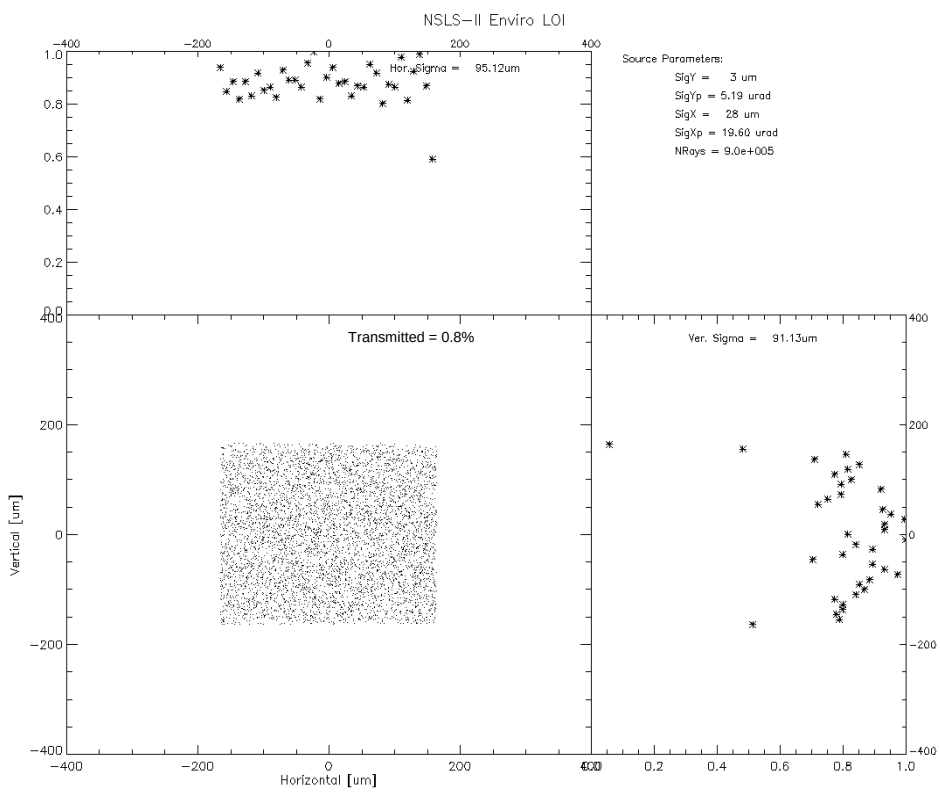

Figure 38. Scatter plot Horizontal optics layout and scatter plots for the ZP beamline with a secondary horizontal source point at 32 m produced by a horizontally focusing mirror.

2.7 List of Major Components

2.7.1 Tabular list of components

Table 2 lists all components for the SRX beamline in their spatial order from source to detector. The distances are in meters relative to center of low-beta (short) straight section. Items in *italics* are for the second canted ZP-branch, which is not in the original scope. A detailed description of key components will follow this table.

Table 2: List of Components for SRX Beamline.

Item	General	KB-branch	*ZP-branch*	Center pos.	Beam sep.
CD 1	Canting Dipole 1				
IVU 22			*Undulator IVU22*	- 1.0 m	
CD 2	Canting Dipole 2			0.0 m	
IVU 21		Undulator IVU21		1.0 m	
CD 3	Canting Dipole 3				
SGV	Slow Gate Valve			15.77 m	31.5 mm
FDAM	Fixed Dual Aperture Mask			16.41 m	32.8 mm
FEXBPM	Front End X-ray Beam Position Monitor			17.4 m	34.8 mm
GBC 1	Gas Bremsstrahlung Collimator 1			18.0 m	36.0 mm
PS-ZP			*Photon shutter*	18.835 m	37.47 mm
PS-KB		Photon shutter		19.4 m	38.8 mm
FGV	Fast Gate Valve			20.2 m	40.4 mm
ALA	Adjustable L Aperture			22.1 m	44.2 mm
GBSS	Gas Bremsstrahlung Safety Shutter			23.35 m	46.7 mm
	Ratchet Wall			24.625 m	
GBC2	Gas Bremsstrahlung Collimator 2			23.9 m	48.1 mm
	FOE Front Wall			25.5 m	
FOE-GV1	First Optical Enclosure – Gate Valve 1			25.57 m	51.2 mm
FOE-B1	FOE Bellows 1			25.71 m	51.6 mm
DV1	Diagnostic Vessel 1			26.13 m	
ZP-WBS			*White beam slits*	26.18 m	52.4 mm
FOE-B2	FOE Bellows 2			26.54 m	53.1 mm
ZP-HMP			*Horizontal mirror pair*	1st 26.745 m 2nd 26.865 m	53.6 mm center line
FOE-B3	FOE Bellows 3			27.02 m	
CLDW	Conductance Limiting Diamond Window			27.14 m	60.72 mm
ZP-DCM			*Double crystal monochromator*	27.9 m	73.2 mm
FOE-B4	FOE Bellows 4			28.66 m	88.1 mm
ZP-BPM1			*Beam Position Monitor 1*	28.82 m	91.7 mm
ZP-WBES			*White Beam End Stop*	28.97 m	93.5 mm
GBC3	Gas Bremsstrahlung Collimator 3			29.22 m	100.7 mm
FOE-B5	FOE Bellows 5			29.48 m	102.8 mm
ZP-BPM2			*Beam Position Monitor 2*	29.665 m	107.3 mm
ZP-SHSA			*Secondary Horizontal Source Aperture*	29.89 m	109.2 mm
ZP-SHSV			*Secondary Horizontal Source Viewer*	30.065 m	113.7 mm
FOE-B6	FOE Bellows 6			30.2 m	115.8 mm
KB-WBS		White Beam Slits		30.29 m	119.1 mm

continued…

Table 2: List of Components for SRX Beamline *(continued)*

FOE-B7	FOE Bellows 7			30.5 m	121.2 mm
KB-DCM		Double Crystal Monochromator		31.26 m	133.8 mm
FOE-B8	FOE Bellows 8			32.02 m	173.6 mm
KB-BPM1		Beam Position Monitor 1		32.18 m	177.2 mm
KB-WBES		White Beam End Stop		32.33 m	179.0 mm
GBC4	Gas Bremsstrahlung Collimator 4			32.58 m	186.2 mm
FOE-B9	FOE Bellows 9			32.84 m	188.3 mm
KB-BPM2		Beam Position Monitor 2		33.025 m	192.8 mm
KB-HS		Horizontal slit		33.325 m	197.3 mm
FOE-BP1	FOE Beam Pipe 1			33.623 m	205.3 mm
FOE-B10	FOE Bellows 10			33.905 m	207.5 mm
KB-HFM		Horizontally focusing mirror		34.8 m	222.5 mm
FOE-B11	FOE Bellows 11			35.695 m	244.5 mm
FOE-BP2	FOE Beam Pipe 2			38.378 m	365.1 mm
ZP-PS			*Photon Shutter*	41.0 m	365.1 mm
KB-PS		Photon Shutter		41.6 m	379.0 mm
	FOE End Wall			41.9 m	385.9 mm
	Shielded Beam Pipes				
	ZP Endstation Front Wall			45.8 m	475.6 mm
ZP-BPM3			*Beam Position Monitor 3*	49.0 m	549.2 mm
ZPL			*Zone Plate*	50 m	572.2 mm
ZP-SS			*Sample Stage*	50.8 m	574.0 mm
	Endstation Mid Wall			52.8 m	
KB-BPM3		Beam Position Monitor 3		53.5 m	
KB-SHSA		Secondary Horiz. Source Aperture		53.6 m	
KB-SHSV		Secondary Horiz. Source Viewer		53.7 m	
SMKBV		Vertical KB mirror		56.23 m	
SMKBH		Horizontal KB mirror		56.42 m	
KB-SS		Sample Stage		56.5 m	
	KB Endstation Rear Wall			58.5 m	

2.7.2 Detailed description of key components

Note: The optical components of the ZP branch are listed in *italic* to distinct quickly between the two branches.

Canting Dipole 1 (CD1)

This is an electromagnet dipole designed to steer the beam 1 mrad outboard. It will work in series with two additional dipoles - CD2 (2 mrad inboard) and CD3 (1 mrad outboard) - together providing the angular deflection required to separate the center line of the KB and ZP branch and bringing the electron beam back to the uncanted straight section centerline. The three dipole magnets will likely operate from a common power supply in series resulting in a zero deflection summation. The exact location, the bending radius and/or the field length need to be defined so that accurate source locations and center lines can be determined for the ZP and KB branch. For example, the ZP undulator source for raytacing purposes would effectively originate from the center of CD1

deflecting the beam outboard from this point 1 mrad. With CD2 located at the center of the low beta straight, the horizontal location of the KB source would be displaced outboard by the distance between CD1 and CD2 times 1 mrad. With the upstream end of the ZP undulator approximately -1.75 m from the center, it can reasonably be estimated that CD1 would be located about -2 m from CD2, resulting in an outboard horizontal displacement of 2 mm for the KB branch source. Therefore for synchrotron raytracing purposes the KB branch source would originate at an X = 2 mm and Z = 0 mm deflected inboard from this point by 1 mrad. Note that there will be a small correction for the outboard horizontal displacement of the KB branch that will depend on the bending radius of CD1.

Zone plate branch undulator
The discussion over the properties of this device is still ongoing. The goal is to have a full coverage of x-ray energies extending from just below the phosphorous K – absorption edge up to approx. E = 15 keV. The ZP source ray originates at the intersection of a ray making a 1 mrad outboard angle with the straight section centerline and the tangent to CD1 bending radius.

Kirkpatrick-Baez mirror branch undulator
The KB branch in-vacuum undulator is optimized to allow access on the 3rd harmonic to just below the titanium K – absorption edge as well as to minimize drop offs at harmonic transition points. It will be extremely important to control the upstream and downstream gap of this device precisely and reproducibly to 0.5 micron. The development of the motion control of this device will be a significant technical challenge. The ultimate goal is to be able to scan the undulator and monochromator synchronously maintaining the monochromator alignment with the undulator harmonic to better than 1 % or (depending on harmonic used) from around 1 to 5 microns gap accuracy. One possible approach is to design and install before the FOE WBS (see below) a real-time energy monitor that intercepts a horizontal edge of the undulator fan. This real-time energy monitor consisting of a channel cut crystal and photo diode could be operated in a phase locked loop that constantly determines the peak energy of the harmonic. Once calibrated (with aperture dependent offsets) the monochromator crystal angle can be slaved to its output. This control approach places the more difficult to control device – the undulator – as the master. Energy scans would be performed – on the fly – by driving the undulator along a gap speed time trajectory. It is recommend to leave space in the FOE layout between the shield wall and FOE WBS for such a device.

Fixed Dual Aperture Mask (FDAM)
This is a fixed dual missteer, power limiting and differential pumping aperture. Centered on each branch is a rectangular 20 sigma divergence aperture with a size at 16.41 m of 6.56 x 1.64 mm^2 (H x V). It will act to protect downstream components in case orbit control loss as well as limit the total power delivered to downstream components. It will also act a conductance limiter and together with upstream and downstream pumps should achieve about three orders of magnitude of differential pumping. The aperture size is dictated mostly by requirements for initial beam alignment. Once a good orbit is established a much smaller aperture could be used. By combining this dual fixed aperture with adjustable “L” apertures both, initial orbit control can be established and the power delivered to the FOE can be greatly reduced. The actual size of this slit will be dictated by the machine physicist’s requirements for initial orbit control.

Front End X-ray BPM (FEXBPM)
This x-ray BPM will be used to adjust and stabilize the orbit by feeding back to storage ring trim magnets. These devices and their control systems are in the domain of the machine physicists. One set will be needed for each undulator. It’s not clear up to now if there will be a set of trim magnets for each undulator – they may operate in an either or mode.

Gas Bremsstrahlung Collimator 1 (GBC1)
This in-air gas bremsstrahlung collimator will consist of lead blocks arranged around a rectangular beam pipe with a lead length along the beam of 300 mm. The ID of vacuum beam pipe is 51.2 x 9.8 mm (H x V). Allowing for a 3 mm wall thickness the ID of the lead collimator is 58 x 16 mm (H x V). The outside dimensions of the collimating blocks must overlap the inside dimensions of the GBC2 located inside the ratchet wall. Since this is an in air

collimator its aperture must in the horizontal encompass the separation of the two branches resulting in a wide aperture. When a full GB study is performed for the beamline it will be worth considering breaking this collimator up to two parts. The first part would be a in vacuum tungsten collimator with two holes sized to be 3 mm all around larger then the extremal ray of the missteered beam at the collimator location. The second part would be an in air lead collimator with an ID that overlaps the OD of the first collimator and who's OD overlaps the ID of the ratchet wall collimator (GBC2). This would result in a much greater collimation potentially simplifying the collimators and stops needed in the FOE.

Photon Shutter ZP and KB (PS-ZP and PS-KB)
These are movable glancing incidence thermal stops capable of absorbing the full power passed by either the ZP aperture or the KB aperture in the FDAM. They will allow either the KB or the ZP branch beam to pass.

Fast Gate Valve (FGV)
This gate valve is design to protect the ring vacuum should there be a failure of the downstream vacuum. It will be triggered by both, a beamline vacuum fault and a front end vacuum fault. Both PS-ZP and PS-KB would rapidly close together with this valve. The storage ring RF should not need to be tripped as long as the ring vacuum stays in acceptable limits.

Adjustable L Apertures (ALA)
A pair of these adjustable L apertures will be centered on each branch. When fully open they will act as a synchrotron missteering mask and when closed they will have a -4 mm overlap. The main purpose of these adjustable masks is to reduce the size of the beam passed to the FOE to a minimum required by the x-ray optics. Typically they will be set slightly larger than the precision FOE white beam slits. By reducing the power absorbed by the FOE white beam slits to a minimum the stability of these precision slits will be greatly improved.

Gas Bremsstrahlung Safety Shutter (GBSS)
The present proposal is to build this shutter out of a pair of in-air lead blocks each 300 mm long mounted on separate vertical actuators (redundant shutters). The blocks are connected in the direction of the beam to hollow beam tubes and bellows that allows the beam to pass when the blocks are lower and the bellows flexible enough to allow the blocks to be moved into the gas bremsstrahlung fan. The OD of the lead blocks will over lap the ID of ratchet wall GBC2.

Gas Bremsstrahlung Collimator 2 (GBC2)
This in-air gas bremsstrahlung collimator will consist of 300 mm long lead blocks arranged around a rect-angular beam pipe that passes through the ratchet wall. The upstream edge of this collimator starts at the upstream edge of the ratchet and it is built into the wall. The ID of vacuum beam pipe is 65.8 x 10.4 mm^2 (H x V). Allowing for a 3 mm wall thickness the ID of the lead collimator is 71.8 x 16.4 mm^2 (H x V).

Diagnostic Vessel 1 (DV1)
Located upstream in the vessel will be an outboard and inboard port for mounting the ZP and KB branch undulator harmonic energy monitor. Downstream will be the ports for mounting the horizontal and vertical ZP branch white beam slits.

ZP White Beam Slits (ZP-WBS)
These slits are of the relative open and center type allowing a preset aperture to be scanned across the beam. The upstream edges water-cooled copper wedges backed on the downstream edge with a beam defining tungsten edge. The resolution and repeatability for the centering stage should be 0.1 µm with a range of +/- 3 mm. The relative opening stage should have a resolution and repeatability of 0.1 µm and a maximal opening of 10 mm.

ZP Horizontal Mirror Pair (ZP-HMP)

The ZP-HMP is located as close as possible to the shield wall in the FOE. It will both, deflect the beam horizontally outboard and thus create a beam separation at the endstation, and form a secondary horizontal source (SHS) that can be manipulated by a secondary horizontal source aperture (SHSA). The center of the ZP-HMP is located at 26.78 m. The mirror pair focuses the horizontal source with a demagnification of 9 at 29.89 m. The ZP-HMP will be compact since the coherent horizontal divergence is low (4.1 μrad), requiring only 120 μm optical aperture (OA). The mirrors will be water cooled silicon, each half coated with rhodium and operating at a fixed incident angle of 4 mrad for a total horizontal deflection of 16 mrad. The second mirror will have a dynamic bender that will correct for the thermal bump on the first mirror and focus the beam to approximately 7 μm FWHM at the SHSA. Each mirror will be 110 mm long (separated by 10 mm) with an optical aperture of 70 mm, a thickness of 30 mm and 25 mm wide. A water-cooled copper mask located on the upstream leg of the first mirror (travelling with the mirror pitch and height displacement) will protect the mirrors from the normal incidence beam as well as shadow all the support and bender components downstream. This mask will also have an aperture to allow the KB branch beam to pass inboard of the backside of the mirrors. The mask will have a copper edge leading to the optical surface. The total horizontal travel will be limited to +2mm and -4 mm. A 10 mm vertical displacement of both mirrors together, will move the beam between the rhodium and the silicon stripe. The ZP branch centerline is now deflected an additional 16 mrad outboard.

Conductance Limiting Diamond Window (CLDW)
This is a diamond window mounted inside a movable water-cooled copper frame. When the window is in the beam the copper frame makes a small gap with a stationary frame. The small gap acts as a differential pump The main function of the CLDW is to help isolate potential poor vacuum from the upstream optics and storage ring vacuum. Both branches with travel through this window.

ZP Double Crystal Mono (ZP-DCM)
This is an indirectly LN_2 cooled Si (111) double crystal monochromator that bounces the beam down 25 mm with an energy range of E = 2.1 keV to E = 15 keV (the incident angle ranges thus from 70 to 7 deg). It will allow the KB branch beam to pass 73.2 mm inboard in a common vacuum.

ZP Beam Position Monitor 1 (ZP-BPM1)
This beam position monitor is for setup and alignment only. During operation it will be moved to an open aperture. This BPM will be mounted on a vertical through-vacuum actuator in a four way cross. In the outboard horizontal port will be a window that will allow a CCD camera to image on the BPM screens. In the lower outboard corner will be an eclectically isolated tungsten blade mounted through a ceramic insulator to a water-cooled copper mask. This tungsten blade will allow measuring the total beam current striking it and can be used to center the upstream white beam slits, the mirrors and the monochromators 1st crystal on the white beam. Just above the tungsten blade will be a diamond scintillation screen. This screen will allows to view the white beam and will also aid in alignment of upstream slits mirrors and monochromator first crystal. Both, the tungsten blade and the diamond window, should be wide enough to intercept the beam off one or both mirrors. Offset vertically by 25 mm and centered on the double mirror defected beam centerline will be a doped YAG screen that will allow us to optically monitor the diffraction condition of the monochromator second crystal. Two apertures above the diamond screen and the YAG screen will allow the white / pink and monochromatic beam to pass by translating the actuator down 10 mm.

ZP White Beam End Stop
This water-cooled, wedged copper block will be capable of absorbing the full white beam power passed by the FDAM. This thermal stop will be mounted in the same vacuum vessel as the in-vacuum tungsten GBC3. It serves to protect the tungsten GBC.

Gas Bremsstrahlung Collimator 3 (GBC3)
This in-vacuum 200 mm long tungsten block will block the GB fan and will have a hole aligned with the double mirror deflected monochromatic beam.

ZP Beam Position Monitor 2 (ZP- BPM2)
This is a thin foil back fluorescence quad diode BPM. It will provide vertical and horizontal beam position information that will allow the mirrors and the monochromator optics to be stabilized with a feedback loop. It will have six apertures on a rotary stage to allow up to five different foils to be placed into the beam with the sixth aperture blank.

ZP Secondary Horizontal Source Aperture (ZP-SHSA)
This will be a pair of relative open and center XY-slits. The slit blades will be made of polished tungsten carbide rods. Since these slits will act as the source for the ZP optics they must be extremely stable both to vibration and long period drifts.

ZP Secondary Horizontal Source Viewer (ZP-SHSV)
Located just downstream of the ZP-SHSA will be a removable YAG screen. The screen will be mounted with a 45 degree pitch relative to the beam and a re-entrant tube with a glass window will allow a long working distance CCD microscope with 20x magnification to view the beam focus. This visual system is crucial for beamline alignment and horizontal focus optimization.

KB White Beam Slits (KB-WBS)
These slits are identical to the ZP-WBS with the ability to allow the outboard ZP beam to pass.

KB Double Crystal Monochromator (KB-DCM)
This is a vertical axis double crystal monochromator that offsets the beam inboard by 25 mm. It will have three indirectly LN_2 cooled crystals, a Si (111), Si (311) and a place holder for a multilayer. Its energy range will be from E = 4.1 keV to E = 28 keV.

KB Beam Position Monitor 1 (KB-BPM1)
This beam position monitor is for setup and alignment only. During operation it will be moved to an open aperture. This beam will be mounted on a vertical through vacuum actuator in a four way cross. In the inboard horizontal port will be a window that will allow a CCD camera to image on the BPM screens. At the lower edge of the BPM will be an eclectically isolated tungsten blade mounted through a ceramic insulator to a water-cooled copper mask. This tungsten blade will allow measuring the total beam current striking it and can be used to center the upstream white beam slits and monochromator first crystal on the white beam. Just above the tungsten blade will be a diamond scintillation screen. This screen will allow viewing the white beam and will also aid in alignment of upstream slits and the first crystal of the monochromator. Offset horizontally inboard by 25 mm will be a doped YAG screen that will allow optically monitoring the diffraction condition of the second crystal of the monochromator. Translating the actuator up by 10 mm will remove them from beam.

KB White Beam End Stop
This water-cooled, wedged copper block will be capable of absorbing the full white beam power passed by the FDAM. This thermal stop will be mounted in the same vacuum vessel as the in-vacuum tungsten GBC4. It serves to protect the tungsten GBC.

Gas Bremsstrahlung Collimator 4 (GBC4)
This in-vacuum 200 mm long tungsten block will block the GB fan and will have a hole aligned with the monochromatic beam.

KB Horizontal Slit (KB-HS)
These are the same as the ZP-SHSA but without the vertical slit.

KB Horizontally Focusing Mirror (KB-HFM)
The KB monochromator illuminates a 1.2 m long water-cooled silicon horizontally focusing mirror (HFM) half coated with rhodium and operating at a fixed incident angle of 2.5 mrad. The HFM is located at 34.8 m and deflects

the beam inboard by 5 mrad forming a secondary horizontal focus at 53.6 m with a demagnification of 1.85. The KB line beam passes by the ZP line endstation experimental table approxi-mate 0.5 m inboard contained in a narrow profile shielded transport pipe

KB Secondary Horizontal Source Aperture (KB –SHSA)
This is the same as the ZP-SHSA.

KB Secondary Horizontal Source Aperture (KB –SHSV)
This is the same as the ZP-SHSV.

SMKB Vertical Mirror (SMKBV)
The vertically focusing optics plan exploits the low vertical divergence of the source by utilizing a single 280 mm long vertically focusing mirror at 56.23 m. This mirror is capable of collecting nearly the full vertical source divergence and focusing it 270 mm away to a focal spot of 70 nm with a divergence of 2.5 mrad.

SMKB Horizontal Mirror (SMKBH)
The secondary horizontal focus is re-imaged by a 100 mm long horizontal KB mirror with a focal length of 80 mm, a demagnification of 35 and a divergence of 3 mrad.

3 END STATION INSTRUMENTATION

3.1 Hutch Mechanical, Environmental and Utilities Requirement

The experimental hutch of the high energy SRX-KB branch will be a monochromatic beam enclosure with its upstream wall positioned at 52.8 m from the second canting bend source point. This wall is shared with the lower energy SRX-ZP experimental hutch that sits upstream (Figure 7). The end wall of the SRX-KB hutch is designed to sit at 58.5 m. There are a number of mechanical, engineering, and utility requirements that are both generally and specifically necessary to support the user science program at the beamline and to ensure optimal instrument stability and performance. The hutch should be designed with the following:

- *User and Equipment Access*: Convenient access needs to be provided to support both beamline and user instrumentation that will be utilized at this station. Access to the SRX-KB hutch should be through sliding doors which are double width for equipment and single capability for personnel. The roof of the enclosure should be surrounded by a railing to permit safe personnel access and there should be convenient access to the roof areas via access ladders to permit equipment installations. Precise positioning and remounting of equipment within the hutch should be provided through the placement of laser tracked floor and wall fiducials. A number of experiments will likely require interfacing between permanent beamline instrumentation and user equipment. Setup and utilization of such equipment will be significantly enhanced by providing interlocked user labyrinths to allow for easy transfer of equipment cabling out of the hutch without the need to engage floor coordinators. Crane access will also be required, but a mobile crane rather than a fixed overhead system will likely be acceptable and less invasive.

- *Hutch Environment*: The spatial resolution requirements of the instrument will necessitate careful control of hutch temperature, humidity and airflow. Although a careful evaluation of thermal requirements should be modelled, it is reasonable to assume that air temperature control of ± 0.1 °C will be required to limit spatial drift to approximately 10 nm per 1 cm. The hutches should provide baffled airflow to minimize air currents and the "windsock" design that has been implemented at PETRA III for their experimental endstations has high merit as an implementable design here. Deviations in hutch temperature and humidity would also be likely minimized by providing airlocked access to the hutch. Airlocks on the hutch access doors, however, are potentially cumbersome to implement and could prove a nuisance for frequent user access to the hutch. An alternative is to provide an environmentally controlled user-control cabin, which is accessed through an airlock that shares similar environmental parameters as the hutch. The hutches need to provide particulate filtering (possibly HEPA filtering for the instrumentation area) for air entering the hutch. It is also anticipated that some experimental work will involve the analysis of manufactured nanomaterials, which will likely require HEPA filtering on air outflow for safety.

- *Signal and Utilities requirements:* There are a number of specific signal and utilities requirements for the SRX beamline that need consideration. A liquid N_2 tap must be provided for cooling detectors and the sample cyro-stage. It is desirable to utilize SEMIFLEX/Triax type delivery systems to deliver low pressure liquid nitrogen so that no gas is vented through the equipment. A chilled water panel should be provided to cool electronics and temperature sensitive experimental cells supplied by users. A compressed air panel nominally rated at 75-100 psi pressure for pneumatic valves and devices will likely be required for equipment shutters that may be utilized in XRD applications, etc. Video monitoring of the hutch and sample via Ethernet CCD camera systems will be required (i.e. high-speed CCD's). Hutch monitoring should utilize pan-tilt-zoom systems. It is also required to have access to various standard signals for monitoring beam position and intensity, but also have requirements specific to the nature of this experiment. A signal patch panel into the hutches must be provided that should be configured to allow for multiple plugin of:
    - BNC connectors (estimate 32, required for beam position readout, binary I/O, TTL, etc.)
    - Lemo (estimate 32, similar equipment need as BNC)

- HV (estimate 8, for providing clean power to ion chambers and detectors, many of these HV supplies will be in the hutch, but it's prudent to allow for some externally powered equipment outside of the hutch), We would reiterate here the need for clean power to maintain high precision focus on beamline optics.
- RS232 (minimally 8, required for serial devices)
- RJ45 and fiber optic (connector types to-be-determined) ethernet connectors (estimate 16, required for modern detector interfaces and high speed CCD's).

An experimental gas farm and station patch panels with flowmeters must be provided minimally to supply high purity He, N_2, Ar gases.

3.2 Sample Mounting, Environments and Manipulation

The types of samples required for the anticipated scientific applications are variable and therefore the specimen mounting, environment and manipulation apparatus must have flexibility. This flexibility will greatly challenge the design of an instrument with high performance and ease of use.

It is likely that the majority of the experiments will operate at the highest available spatial resolution and that specimen sizes will necessarily be small (~mm) compared to those typically used at currently operating x-ray microprobes (~cm). Nonetheless, it is critical that the SRX-KB probe provide sufficient flexibility to accommodate high-impact experiments that will require relatively large specimens (~cm) and large travel dimensions (~cm). The instrument must accommodate the following sample types:

- Microtomed and Focused Ion Beam (FIB) milled sections: This category includes both geological and biological specimens. While many can be accommodated on TEM grids and SiN windows, biological specimens may require several millimeters of scanning range. Examples include plant specimens (sections of roots, stems, seeds, and leaves with ~mms cross sectional dimensions) and sections from higher order organisms (i.e., human tissue sections, transgenic mice sections). Accommodating sections that are up to 25 mm in diameter is required.
- Individual sub-micron particles: These specimens will likely be mounted on TEM grids or Si3N4 windows.
- Dispersed powders: Traditionally these samples are mounted on Kapton, Mylar, and polypropylene films, but will likely be prepared on TEM and Si3N4 substrates here for higher substrate stability. Some particulate matter will be on filters, such as aerosol collectors, that cannot be easily removed from the collection material.
- Mineral chip polished mounts: These specimens are epoxy embedded polished mounts or polished chips mounted to pure silica glass slides. Accommodating mounts up to 25 mm rounds is required
- Rock and soil thin sections: These are 30 µm standard thickness, mounted on high purity silica slides (i.e., Suprasil). At the smallest size these can be mounted on 25 mm diameter rounds, but conventional rectangular sections are mounted on glass with dimensions of 27 x 46 mm2.
- Intact geologic and biologic specimens: Some specimens will need to be studied whole without sectioning, primarily geological and biological samples for fluorescence microtomography imaging. These samples are large enough to allow element distributions to be determined rather than only bulk compositions (as for sub-micron particles). Typical dimensions will be in the 0.1 mm to 1 mm range.

A variety of sample environments is required to optimize the trade-offs between low-energy x-ray detection, accommodation of water-bearing samples and reduction of photochemical beam effects. Specimen compartment(s) should be available that operate in air, helium or vacuum. Cryogenic capability (down to LN_2 temperatures) will be required for many biological and wet geological materials (such as soils) to minimize radiation damage. Such damage can alter chemical speciation, for example. This capability will probably be best implemented through a cold finger approach. Such systems are being commercially developed (e.g., Xradia) but some facility R&D will likely be required to develop a customized apparatus. High temperatures (up to 1300K) are also of interest in

studying fluid inclusion above homogenization temperatures, for example. However, it remains to be seen if this capability can be implemented without compromising the performance of the instrument for the "mainstream" experiments. Humidity control may also be desirable. One of the big challenges is to design environmental chambers where the specimen can be viewed optically, at least at some moderate magnification (~100x) for analysis targeting purposes. Higher magnification viewing is probably unnecessary because coarse x-ray imaging can provide this targeting guidance. Reasonable sample exchange time (~10 mins) is also desirable with multiple sample cassettes being used where possible and feasible.

The sample mounting assembly needs to incorporate motorized stages that are capable of translating samples with high precision vertically (Y), horizontally (X, inboard-outboard), along the direction of the incident beam (Z, upstream-downstream), and of rotating samples about the focal point (θ). Because of the requirement for a relatively wide range of sample sizes, the motion requirements are best accomplished using a dual, coarse-fine motor stack. The underlying coarse stack will use high resolution linear motors (2 cm travel; 100 nm resolution) whereas the overlying fine stack uses nano-positioning devices (20 μm travel; 10 nm resolution). It will be necessary for the coarse stack to maintain 10 nm stability when stationary (i.e., high rigidity).

Existing, mirror-based hard x-ray microprobes, most commonly have utilized an instrument geometry that places the sample surface at 45° to the incident beam with the detector at 90° to the incident beam. This geometry is optimum for minimizing background from scattered radiation and maximizes space for ancillary equipment, such as optical microscopes. However, it is likely that the focusing optics that will be used to achieve the targeted spatial resolution for the SRX-KB instrument will have reduced working distance to the sample. Additionally, the desire to collect larger solid angles of fluorescence given the likely choice of energy dispersive detector that has been identified for this instrument will also make a 45° sample geometry non-optimal. Consequently, the SRX-KB instrument will be designed to work primarily in normal incidence. In addition to allowing the greatest beam demagnification, this approach will reduce the horizontal footprint of the beam on the sample and place the microscope optic axis coincident with (or at least parallel to) the x-ray beam.

Fluorescence microtomography applications will be accommodated using a high precision rotation stage (0.01°) with the rotation axis aligned with the focal point of the beam. With this rotation stage placed between the fine and coarse x-y-z translation stacks, the fine stages can be used to center the specimen on the rotation axis and for translations during data collection. Another approach is to have the rotation stage as the topmost stage in the fine stack and allow sufficient vertical space for mounting a small goniometer head. The horizontal translations need to account for the full horizontal travel of the sample through the beam to generate a sinogram using the first generation (pencil-beam) approach. For low density biological specimens that are being imaged for emission lines above 12 keV, self-absorption can be corrected for samples that are greater than 1 mm in diameter. Thus, at least 1 mm, high precision (10 nm), horizontal translation will be required for this application.

Next generation experiments utilizing the BNL-CSIRO MAIA detector system will dominantly operate in a continuous scanning mode. As currently designed, this system interfaces with stage motion control in one of two modes. One is an event driven modality where the detector drives the stage directly. The other modality reads the encoder position of the stage as it is being scanned. Both modes of operation are required, thus encoder-enabled stages and controllers are required. Stage scan rates must be able to achieve 1-10 mm/second.

The sample mounting, environment and manipulation requirements cover a fairly wide range of requirements. However, these requirements can be largely met with a few specialized modules which will be designed to be exchangeable on an experiment basis using a fiducial registry system. We envision the following modules listed in order of development:
Module A: Designed for highest flexibility in terms of sample mounting and sample size. Will operate in air and thus will be best suited for initial commissioning and work with high energy fluorescence lines (≥ 5 keV).
Module B: Designed for highest spatial resolution on small samples (TEM grids, FIB sections). Will have helium gas environment to allow efficient detection of low energy fluorescence lines (e.g., down to Al).

Module C: Similar to Module B but with cryogenic capability and vacuum environment. Designed primarily for studies of biological specimens. Likely will not have optical viewing.
Module D: High temperature module with heating stage designed primarily for fluid inclusion work.

3.3 Detectors

The KB branch will be optimized for sub-micrometer x-ray fluorescence imaging, spectroscopy and diffraction. Our choices for detectors at this early design stage reflect our desires to foster and develop next generation data acquisition approaches that best utilize the unique characteristics of the instrument. These approaches include:

- Detectors and spectroscopy amplifiers capable of rapid on-the-fly x-ray fluorescence acquisition. This is requires to allow for imaging of large sample areas while maintaining high pixel resolution and to minimize radiation dose to photo-redox sensitive samples.
- Spectroscopy amplifiers that can provide near real-time elemental analysis will be required due to the large data sets such scans will produce. Even moderately sized datasets can be expected to be tens or hundreds of Gigabytes in size, which are generally unmanageable by users utilizing current consumer level computers and data storage options.
- Imaging mode spectroscopy will likely be the manner in which most near edge spectroscopy data is collected. This has the benefit of allowing for more unambiguous evaluation of differences in speciation at the sub-micron scale. Efficient detectors capable of rapid data collection, with high throughput and large solid angles are required. Typically this capability is best achieved with detector arrays.
- Tomographic fluorescence, absorption and diffraction imaging will be high demand analytical techniques. Rapid fluorescence detectors are required, but additionally calibrated photodiodes with high sensitivity to measure absorption through the sample are needed as well as high sensitivity and rapid readout CCD area detectors for diffraction imaging and tomography.
- Sub-micrometer x-ray diffraction analysis has also become a high demand technique on hard x-ray microprobes, it can be estimated minimally 20% of users will wish to utilize the instrument's spot and imaging XRD capabilities. High sensitivity, low noise area detectors will be required with relatively large 2q coverage and along-beam adjustable position for optimizing angular range and phase-contrast

Considering detector technologies that are either currently available or in advanced stages of development, the following specific systems should be considered for the beamline at a minimum:

- Silicon-drift Detector Array: Multi-cathode detectors area variant of silicon drift diode detector technology. SDD detectors are becoming increasingly popular choices for synchrotron x-ray fluorescence analysis as the technology for SDD detectors has greatly improved over the past few years. While more conventional lithium-drifted silicon (Si(Li)) or high-purity germanium (HPGe) offer substantial x-ray efficiency for a wide range of x-ray energies, they do have their drawbacks, such as the physical limitation due to the presence of a large LN2 dewar attached to the detector. SDD systems, by contrast, operate efficiently at near room temperature yielding a much more compact and flexible system. Another disadvantage of conventional Si(Li) and HPGe detectors is that their capacitance is relatively high, which limits their use at short peaking times and high count rates, and thus are not optimal for the fast scanning modes we wish to develop at SRX-KB. The SDDs, by contrast, exhibit extremely low capacitance (~0.06 pF) and very low leakage current (~10-9 A) due to the unique structure and small anode size, virtually independent of the detector area, providing a system with high throughput and very good energy resolution even when operated at extremely short peaking times. The 4-element multi-cathode X-ray detector arrays are also available featuring large active area per element (~50 mm2) and excellent energy resolution. The detector system will incorporate 4 preamplifiers, one 4-channel digital pulse processor (DPP), power supplies necessary to operate the full spectrometer, an electronic crate for the 4-channel DPP), PCI interface cards and fiber optic communication cables. The DXP spectrometers offer full spectrum or multi-SCA acquisition at sub-millisecond dwell times, which supports the beamline requirement for fast on-the-fly scanning. In mapping mode assuming 1 msec dwell times, the 4-element array will stream full channel spectra

at about 32 Mb/second. The cPCI bus is rated to stream up to 50 Mb/sec. This translates into 113 Gb per hour. Assuming round the clock data collection, storage will be required for up to 2.7 Tb per day.

- Maia detector array: The Maia large solid angle Si detector array is a joint BNL/CSIRO development which utilizes an alternative data acquisition strategy that uses a multiparameter approach in which each photon event is tagged by sample XY position and detector identity and then streamed as 'events' for further processing or storage. The advantage of this strategy is that it exhibits zero read-out overhead and enables faster raster scanning, again, very much in line with the desired performance characteristics of SRX-KB. The Maia system allows complex full-spectral SXRF data to be decomposed into elemental components using a matrix transform method called Dynamic Analysis which in a mature form will permit its execution on the event stream in real-time, again…a desired capability for the beamline. Physically, the Maia utilizes a large planar monolithic silicon detector array and dedicated application specific integrated circuits (ASICs) for signal processing offering large solid-angle collection and high count rates spread over a large number of detectors. A 96 element version of the Maia is currently in commissioning at the NSLS microprobe beamline X27A and at the AS microprobe beamline 5ID and a 384 element final design is in construction for both facilities. Tests at NSLS beamline X27A using the 96 element prototype demonstrated count rates up to 6 M/s, image sizes up to 4.3 megapixels, and dwell times as short as 0.8 ms (limited by stage speed for 7.5 μm pixels). The 384 element final design minimally will generate 4x larger data streams of ~8 24 M/s. As pileup rejection improves on the detector this will likely be larger since they will be able to operate at higher rates. This translates to data rates of roughly 2 Tb/day with round the clock operation.
- Wavelength Dispersive Spectrometer: There may be analyses that require better resolution in separating fluorescence emissions that overlap strongly when detected using energy dispersive detectors (i.e. overlap of rare earth element L emission lines with K emission lines of Ti, V, Cr, Mn, and Fe). These analyses benefit from wavelength dispersive spectrometers utilizing high-resolution fluorescence analyzer crystals lying in a Rowland circle geometry. Commercial devices do exist that are designed to attach to scanning electron microscope systems. Instruments are also being deleloped specifically for x-ray microprobe use, such as that available at the ESRF's ID21. While some experiments might benefit, these systems do have some significant disadvantages as well in that they are difficult to align, must operate in vacuum and minimally have detection sensitivities 10x lower than what is achievable with energy dispersive spectrometers. Thus while useful for a small subset of experiments, other detector technologies listed above must take priority for this instrument.
- Diffraction Area Detector: Microfocused synchrotron x-ray diffraction has proved to be valuable in the in-situ identification of phases in minute amounts of sample. On microprobes, these instruments generally rely on Bragg techniques with a fixed detector position and monochromatic radiation. Two primary limitations need to be considered in selecting suitable detectors for this application. Increased 2θ coverage is generally provided by placing the area detector slightly offset to the incident beam. This offset provides partial coverage of powder diffraction rings over a larger 2θ range than could be achieved with the detector centered. Additionally, while many samples with large numbers of crystallites within the incident beam are strongly diffracting, many samples require longer dwell times to achieve sufficient sensitivity for phase identification. Image Plate area detectors are very effective in allowing users to identify phases in low abundance since they can be operated with little detriment at very long dwell times, often over periods of hours. Modern CCD based area detectors provide short read-out times (a few seconds) with good signal-to-noise for short exposures (<1 minute) which are needed at SRX-HE for the rapid analyses required for phase mapping and tomography. At highest resolution these CCDs output 8 Mb files. Generally μXRD studies are conducted as single point analyses. However, increasingly there is demand for diffraction imaging analysis integrated with coupled with μXRF imaging. We expect that 1 second readouts would be the shortest exposures that are likely to yield analyzable results. In an imaging mode this would result in data rates of ~ 8Mb/sec and for a relatively small 500 x 500 pixel image would generate 2Tb of data.

4 SPECIAL BEAMLINE REQUIREMENTS

As written in section 3 of this report, there are several special requirements this beamline has to comply with. They are described there in detail, therefore here only found as a bulleted list.

- Air temperature control (± 0.1 °C; 10 nm/1 cm)
- Baffled air flow to minimize air currents
- Particulate filtering (possibly HEPA filtering for instrumentation area)
- Signal patch panel (BNC, HV, RS232, ethernet, etc.)
- Experimental gas farm and station patch panels with flowmeters (He, N2, Ar)
- LN2 tap (detectors, cyro-stage)
- Chilled water panel
- Compressed air
- Video monitoring
- Floor access (mobile rather than overhead)
- Floor fiducials

A significant part of future experiments could deal with materials under extreme environments, especially with radioactive samples. Nuclear fuels, containment and waste management are just a few keywords. Therefore, the beamline should be able to handle this kind of material.

5 FUTURE UPGRADE OPTIONS

Only the KB branch of the SRX beamline is in the original scope of project beamlines at the NSLS-II. It is of course desirable to build up the ZP branch within the same timeframe. The advantages would be from the construction side not to interfere with later user activities at the KB branch and from the experiments side the access to a high resolution station where lower energies and thus important elements such as phosphorus, sulfur and calcium are in reach simultaneously to experiments at the KB branch.

APPENDIX 1: SCHEDULE

This Conceptual Design Report will be finished	September 30,2009.
Work on the Preliminary Design Report will begin	October 1, 2009,
and will be finished	October 1, 2010.
Approval of long-lead time procurement will be given	November 3, 2010.
Work on Final Design Report will start	October 4, 2010.
The final design of major components will be ready	April 14, 2011,
and the full report will be finished	February 7, 2012.
Long lead time procurement will begin	January 11, 2011,
and should be finished	November 5, 2012.
Procurement will start	April 20, 2012,
and should end	August 14, 2013.
Beneficial occupancy of the experimental floor will be possible	February,2012.
Installation will start	February 10, 2012,
and should be complete	January 07, 2014.
Sub-system testing will begin	May 15, 2012,
and will be done	February 03, 2014.
Integrated testing will start	August 19, 2013,
and will finish	May 27,2014.
All beamlines should be available for commissioning	May 27, 2014.

Intentionally blank.

APPENDIX 2: REFERENCE DRAWINGS

The following drawings are provided here for reference:

1 Beamline layout in legal format